

Exact site frequency spectra of neutrally evolving tumors, transition between power laws and signatures of cell viability

Einar Bjarki Gunnarsson¹ Kevin Leder¹ Jasmine Foo²

¹Department of Industrial and Systems Engineering, University of Minnesota, Twin Cities, MN 55455, USA.

²School of Mathematics, University of Minnesota, Twin Cities, MN 55455, USA.

Abstract

The site frequency spectrum (SFS) is a popular summary statistic of genomic data. While the SFS of a constant-sized population undergoing neutral mutations has been extensively studied in population genetics, the rapidly growing amount of cancer genomic data has attracted interest in the spectrum of an exponentially growing population. Recent theoretical results have generally dealt with special or limiting cases, such as considering only cells with an infinite line of descent, assuming deterministic tumor growth, or sending the tumor size to infinity. In this work, we derive exact expressions for the expected SFS of a cell population that evolves according to a stochastic branching process, first for cells with an infinite line of descent and then for the total population, evaluated either at a fixed time (fixed-time spectrum) or at the stochastic time at which the population reaches a certain size (fixed-size spectrum). We find that while the rate of mutation scales the SFS of the total population linearly, the rates of cell birth and cell death change the shape of the spectrum at the small-frequency end, inducing a transition between a $1/j^2$ power-law spectrum and a $1/j$ spectrum as cell viability decreases. We use this insight to propose a simple estimator for the ratio between the rate of cell death and cell birth, that we show to accurately recover the true ratio from synthetic single-cell sequencing data. Although the discussion is framed in terms of tumor dynamics, our results apply to any exponentially growing population of individuals undergoing neutral mutations.

Keywords: Mathematical modeling, cancer evolution, branching processes, exponentially growing populations, site frequency spectrum, infinite sites model.

MSC classification: 92D25, 92B05, 60J85.

1 Introduction

The study of genetic variation driven by neutral mutations has a long history in population genetics [1]. Usually, the population is assumed to be of a large constant size N , and reproduction follows either the Wright-Fisher model (non-overlapping generations) or the Moran model (overlapping generations) [2]. Neutral mutations occur at rate u per individual per generation, and each new mutation is assumed to be unique (the *infinite-sites* model of Kimura [3]). This setup gives rise to a sample-based theory of tracing genealogies of extant individuals backwards in time via the *coalescent*, introduced by Kingman [4, 5]. A popular

summary statistic of genomic data is the *site frequency spectrum* (SFS), which records the frequencies of mutations in a population or population sample. Under the Moran model with neutral mutations, the expected number of mutations found in j cells of a sample of size n is $\xi_j = Nu/j$, and any linear combination of the form $\sum_{j=1}^{n-1} jc_j\xi_j$ with $\sum_{j=1}^{n-1} c_j = 1$ is an unbiased estimator of $\theta := Nu$, the population-scaled mutation rate. Prominent estimators of this form include Watterson’s θ_W [6], Tajima’s θ_π [7], Fu and Li’s ξ_1 [8] and Fay and Wu’s θ_H [9], and these estimators form the basis of several statistical tests of neutral evolution vs. evolution under selection [10]. In this way, the site frequency spectrum has provided a simple means of understanding the evolutionary history of populations from genomic data.

Cancer can be viewed as its own evolutionary process, operating at the somatic level. Cancer initiation is usually understood to be a series of mutational events, that culminates in malignant cells able to proliferate uncontrollably [11, 12, 13, 14]. Such “driver” mutations are complemented by more frequent neutral or “passenger” mutations [15, 16], that have no functional role in the evolution to malignancy, but contribute to the genetic diversity characteristic of cancer [17, 18, 19]. The dominant paradigm of tumor progression has been that of sequential clonal expansion of driver mutations. However, several recent works suggest that a neutral evolution model, under which all driver mutations are already present in the tumor-initiating cell, is sufficient to explain the intratumoral heterogeneity in many cancers, see e.g. [20, 21, 22] and the reviews [23, 24]. A simple test of neutral tumor evolution based on the site frequency spectrum was proposed in Williams et al. [22], which has since generated debate e.g. surrounding its significance level and statistical power (see e.g. [25, 26, 27] with author responses in [28, 29]). The authors of [22] subsequently suggested a Bayesian framework for detecting tumor subclones evolving under selection in [30], and more recent approaches to that problem include Dinh et al. [31] and Caravagna et al. [32]. These works and the surrounding debate are indicative both of the fact that increased attention is being paid to the role of neutral mutations in driving heterogeneity in cancer, and that efforts are just underway to develop robust methods of inferring the evolutionary history of tumors.

While the constant-sized models of population genetics are appropriate for understanding early cancer development in small tissue compartments, exponential growth models are more relevant for understanding long-run tumor progression [33, 34]. In recent years, several works have used different versions of such models to derive the site frequency spectrum of an exponentially growing tumor with neutral mutations. To state the most prominent result, assume a branching process model in which cells divide at rate r_0 and die at rate d_0 ($r_0 > d_0$), and that w neutral mutations accumulate on average per cell division. Define $p_0 := d_0/r_0$ as the *extinction probability* of the tumor (Section 2), and $q_0 := 1 - p_0$ as its *survival probability*. If we consider only cells with an infinite line of descent, and assume the number of cells N is large, the expected number of mutations found in j cells is $\xi_j = (w/q_0)N \cdot 1/(j(j+1))$. This SFS differs from the SFS of the constant-sized Moran model of population genetics in two important ways: The spectrum now follows a $1/j^2$ power law as opposed to a $1/j$ law, and it now depends on the growth parameters r_0 and d_0 via the survival probability q_0 . Versions of the $1/j^2$ spectrum have been established by Durrett [35, 33], Bozic et al. [36] and Williams et al. [22], as we discuss in more detail below. In [22], [36] and [21], the $1/j^2$ spectrum was used to infer the ratio w/q_0 from tumor data, but extracting information about the mutation parameter w and the growth parameter q_0 separately seemingly requires additional tools. In a recent work by Werner et al. [37], the authors measured pairwise mutational differences between the ancestors of spatially separated tumor bulk samples, and they developed a coalescent-based approach for estimating w and a function of p_0 defined in (2) below.

The extinction probability p_0 quantifies the viability and turnover of tumor cells. As cell

turnover increases, the mutational burden and genetic diversity of the tumor increases, which enhances its adaptability under treatment. As a result, it is important to be able to identify tumors with a high cell turnover, i.e. with a large extinction probability p_0 . Prior works on the SFS of an exponentially growing tumor population offer only a limited understanding of how p_0 affects the spectrum, as these works generally only consider cells with an infinite line of descent, or they consider special cases such as deterministic growth of the tumor bulk or no cell death ($p_0 = 0$), which is reasonable when p_0 is small. Moreover, many prior results are given in the large-time or large-population limit, and for practical reasons, the focus is often on mutations of frequency 5 – 10% and higher. These results are discussed in more detail in Section 6. Our goal in this work is to gain a more complete understanding of the SFS of an exponentially growing tumor with neutral mutations. In particular, we seek to understand how the spectrum behaves both at small and large frequencies, for all values of p_0 and the population size N . We obtain separate results for cells with an infinite line of descent and for the total population, evaluated either at a fixed time or at the stochastic time at which the population reaches a certain size, each of which is relevant to tumor data analysis depending on the context. We observe that while the SFS of skeleton cells depends on the mutation rate w and the extinction probability p_0 only via w/q_0 , the two parameters decouple in the SFS of the total population. In fact, as p_0 increases from 0 to 1, the small-frequency end of the spectrum transitions from the $1/j^2$ power law characteristic of pure-birth exponential growth to the $1/j$ power law characteristic of a constant-sized population. We investigate simple metrics that quantify this transition, and we use one of them to propose a simple estimator for p_0 , that we subsequently evaluate using synthetic single-cell sequencing data.

The rest of the paper is organized as follows. In Section 2, we formulate our branching process model with neutral mutations, define the *skeleton* subpopulation of cells with an infinite line of descent, and establish relevant notation. In Section 3, we analyze the SFS of skeleton cells, and in Section 4, we analyze the SFS of the total cell population. In Section 5, we use our theoretical results to propose and evaluate a simple estimator for p_0 . In Section 6, we summarize our results, and discuss in detail how they relate to the existing literature. The proofs of all of our theoretical results are found in appendices at the end of the paper.

2 Model description

We assume that the tumor evolution follows a branching process model. Cells divide into two cells at rate $r_0 \geq 0$ per unit time and die at rate $d_0 \geq 0$ per unit time, which means that in a small time interval of length Δt , a cell divides with probability $r_0 \Delta t$ and dies with probability $d_0 \Delta t$. Assume $r_0 > d_0$ and define $\lambda_0 := r_0 - d_0 > 0$ as the net growth rate. Let $Z_0(t)$ denote the size of the tumor population at time t and assume $Z_0(0) = 1$, i.e. the tumor expands from a single tumor-initiating cell. Define

$$\Omega_\infty := \{Z_0(t) > 0 \text{ for all } t > 0\}$$

as the event that the tumor does not go extinct, and

$$p_0 := \mathbb{P}(\Omega_\infty^c) = \mathbb{P}(Z_0(t) = 0 \text{ for some } t > 0)$$

as the *extinction probability* of the tumor. This probability can be computed as $p_0 = d_0/r_0$ with $0 \leq p_0 < 1$, see e.g. Section 3 of [33]. Note that any clone derived from a single tumor cell gives rise to its own branching process with the same growth parameters r_0 and d_0 and

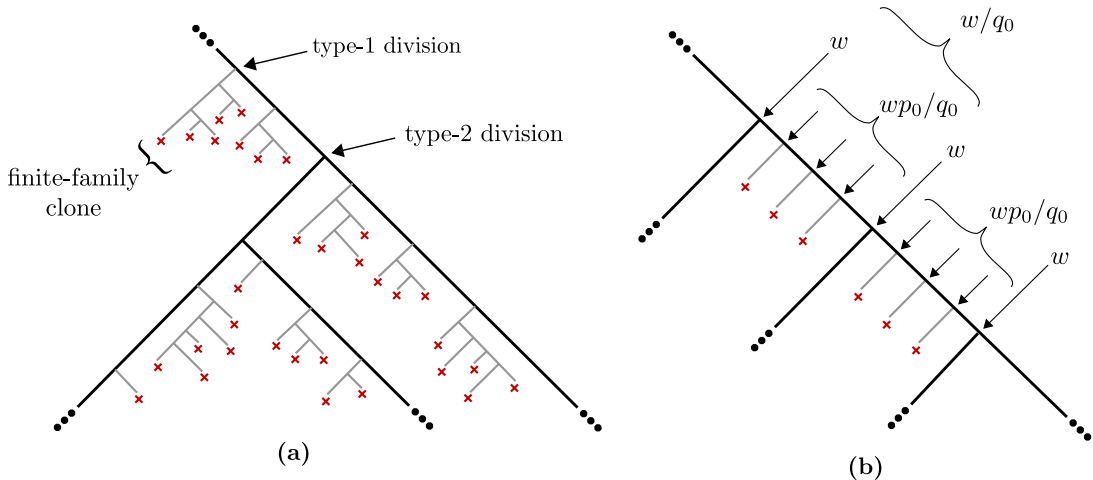


Figure 1: **(a)** The skeleton subpopulation, which consists of cells with an infinite line of descent, can be thought of as the trunk and scaffolding branches of the genealogical branching tree (bold branches). Each skeleton cell divides into one skeleton cell and one finite-family cell at rate $2d_0$ (type-1 skeleton division), in which case a finite-family clone grows out from the skeleton as a lateral branch (light gray branches). Each skeleton cell divides into two skeleton cells at rate λ_0 (type-2 skeleton division), in which case another scaffolding branch is added. **(b)** In between two type-2 skeleton divisions, the expected number of mutations that accumulate on type-1 divisions is wp_0/q_0 . Since w mutations on average are added on each type-2 division, the expected number of mutations per skeleton level is $wp_0/q_0 + w = w/q_0$.

the same extinction probability. We also define

$$q_0 := 1 - p_0 = \lambda_0/r_0 \quad (1)$$

as the *survival probability* of the tumor or a single-cell derived clone. On the nonextinction event Ω_∞ , the cells alive at time t can be split into two categories, one consisting of cells with an infinite line of descent, i.e. cells that start clones that do not go extinct, and the other consisting of cells whose descendants eventually go extinct. We refer to the former cells as *skeleton* cells and the latter as *finite-family* cells. An arbitrary tumor cell is a skeleton cell with probability q_0 , so in the long run, the proportion of skeleton cells in the population is q_0 . We can think of skeleton cells as forming the trunk and scaffold branches of the genealogical branching tree, with finite-family clones growing out from the skeleton as lateral branches, see Figure 1a.

We next add neutral mutations under the infinite-sites model. Prior to a cell division, each parental DNA molecule is unwound and separated into two complementary strands. Each parental strand serves as a template for the construction of a new complementary daughter strand. The end result is two copies of the DNA molecule, each consisting of one parental strand and one daughter strand. Errors in nucleotide pairing during this process can result in one or more point mutations per daughter strand. We assume that these errors amount to $w/2$ mutations on average per daughter strand, for a total of w mutations on average per cell division. We make no assumption on the distribution of the number of mutations apart from its mean. The point mutation rate has been estimated as $5 \cdot 10^{-10}$ per base pair per cell division for normal cells [38], and it is commonly higher in cancer due to genomic instability [17]. Since the number of base pairs is of order 10^7 in the exome and 10^9 in the

genome, it makes sense to allow w to be any positive number, i.e. $w \in (0, \infty)$. In many works, the convention is to allow at most one mutation per cell division, introducing a probability $u \in (0, 1)$ of a new mutation. Since our analysis only depends on the mean number of mutations w per cell division, it includes this case with $w := u$. Finally, while our focus is on the above discrete model of mutation accumulation, we will also present all of our results in terms of continuous mutation accumulation, another common and biologically relevant assumption. In the continuous model, neutral mutations occur at rate $\nu > 0$ per cell per unit time at any time throughout the lifetime of the cell.

Before proceeding, we need to make a distinction between *clonal* and *subclonal* mutations. Say the tumor-initiating cell divides into two cells A and B , and say that cell A acquires a new mutation. If the clone started by cell B eventually dies out, the mutation in cell A will be shared by all tumor cells from that point onward, making it *clonal*. However, if the clones started by A and B both survive, the mutation becomes *subclonal*, i.e. there is always at least one tumor cell without it. While this example demonstrates how clonal mutations can arise post-initiation, all mutations that accumulate prior to cancer initiation, as the cancer precursor cell evolves to malignancy, also become clonal. For this reason, the clonal mutations usually tell us more about the events preceding cancer than the dynamics post-initiation, and they can in fact outnumber the subclonal mutations [15]. Nevertheless, clonal mutations do appear in the SFS of mutations post-initiation, and they play distinct roles in the fixed-time and fixed-size spectrum, which is why we pay them special attention below.

3 Site frequency spectrum of skeleton cells

In this section, we establish the expected fixed-time and fixed-size spectrum of skeleton cells. The reason we are interested in analyzing skeleton cells separately is twofold:

- When $p_0 = 0$ (no cell death), all cells are skeleton cells, and the SFS of the total population is the SFS of the skeleton. More generally, when p_0 is small, the total population spectrum is well-approximated by the simpler skeleton spectrum.
- When the extinction probability p_0 is large, finite-family cells affect the SFS of the total population at the small-frequency end. However, the large-frequency end is still characterized by the skeleton spectrum, as we demonstrate in Section 4 below.

3.1 Effective cell division and effective mutation rate

When the tumor is conditioned on nonextinction, the probability that the tumor-initiating cell divides during the first Δt units of time, and that exactly one of the two daughter cells survives, i.e. starts a clone that does not go extinct, is

$$\frac{\mathbb{P}(\text{division in } [0, \Delta t], \text{ one offspring survives})}{\mathbb{P}(\Omega_\infty)} = \frac{r_0 \Delta t \cdot 2p_0(1 - p_0)}{1 - p_0} = 2r_0 p_0 \Delta t,$$

and the probability of a division in $[0, \Delta t]$ where both daughter cells survive is

$$\frac{\mathbb{P}(\text{division in } [0, \Delta t], \text{ both offspring survive})}{\mathbb{P}(\Omega_\infty)} = \frac{r_0 \Delta t \cdot (1 - p_0)^2}{1 - p_0} = r_0(1 - p_0) \Delta t.$$

Since each skeleton cell starts a clone that does not go extinct, we can conclude that a skeleton cell divides into one skeleton cell and one finite-family cell at rate $2r_0 p_0 = 2d_0$ per unit time

(type-1 skeleton division), and it divides into two skeleton cells at rate $r_0q_0 = \lambda_0$ per unit time (type-2 skeleton division). The probability that a skeleton division is type-2 is

$$\kappa_0 := \frac{r_0q_0}{r_0q_0 + 2r_0p_0} = \frac{1 - p_0}{1 + p_0}. \quad (2)$$

This probability can also be computed directly as follows: $(1 - p_0)^2$ is the probability that both daughter cells survive, and $1 - p_0^2$ is the probability that at least one of them does, so $(1 - p_0)^2/(1 - p_0^2) = (1 - p_0)/(1 + p_0)$ is the probability that a skeleton division is type-2.

Let $\tilde{Z}_0(t)$ denote the number of skeleton cells at time t , conditional on the nonextinction event Ω_∞ . Since type-1 divisions do not affect the size of the skeleton, we can think of the type-2 divisions as the “effective” divisions. More precisely, $(\tilde{Z}_0(t))_{t \geq 0}$ is a pure-birth exponential growth process, or a *Yule process*, with birth rate λ_0 and mean size $\mathbb{E}[\tilde{Z}_0(t)] = e^{\lambda_0 t}$ [33, 39]. Type-1 divisions do contribute to mutation accumulation however. Indeed, each type-1 division adds $w/2$ mutations on average to the skeleton, and each type-2 division adds w mutations on average. The rate at which mutations accumulate on the skeleton is then

$$(w/2) \cdot 2r_0p_0 + w \cdot r_0(1 - p_0) = wr_0 \quad (3)$$

per unit time, which equals the mutation rate for the original, unconditioned process $(Z_0(t))_{t \geq 0}$. The mutation rate per type-2 division, or the *effective* mutation rate, is on the other hand

$$wr_0/\lambda_0 = w/q_0 \quad (4)$$

per unit time. We can also think of w/q_0 as the expected number of mutations that accumulate per skeleton level as follows. Upon a type-2 division, the number of type-1 divisions before the next type-2 division has the geometric distribution with support $\{0, 1, 2, \dots\}$ and success probability κ_0 given by (2). It follows that in between two type-2 divisions, the expected number of mutations that accumulate on the skeleton due to type-1 divisions is

$$(w/2) \cdot (1/\kappa_0 - 1) = (w/2) \cdot 2p_0/q_0 = wp_0/q_0. \quad (5)$$

When we include the type-2 division that starts each skeleton level, we obtain

$$wp_0/q_0 + w = w/q_0, \quad (6)$$

mutations per skeleton level (Figure 1b). The effective mutation rate w/q_0 plays a key role in the SFS of the skeleton, with the continuous-time viewpoint in (4) applying to the fixed-time spectrum, and the population-level viewpoint in (6) applying to the fixed-size spectrum.

3.2 Expected fixed-time and fixed-size skeleton spectrum

Let $\tilde{S}_j(t)$ denote the number of mutations that are found in $j \geq 1$ skeleton cells at time t , conditional on the nonextinction event Ω_∞ . This is the site frequency spectrum of skeleton cells. For any integer $N \geq 1$, define

$$\tilde{t}_N := \log(N)/\lambda_0, \quad (7)$$

as the (fixed) time at which the skeleton has expected size N , i.e. $e^{\lambda_0 \tilde{t}_N} = N$, and define

$$\tilde{\tau}_N := \inf\{t \geq 0 : \tilde{Z}_0(t) = N\} \quad (8)$$

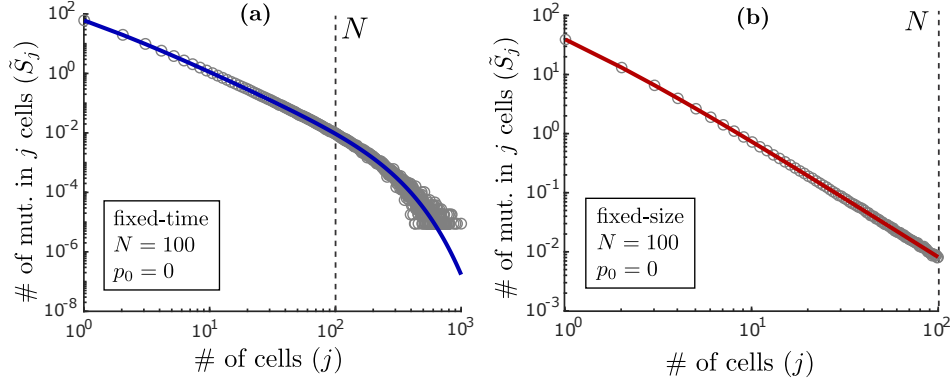


Figure 2: **(a)** The expected fixed-time spectrum (9) of Proposition 1 (solid blue line) shows good agreement with the average spectrum of simulated tumors (grey dots) for the parameters $N = 100$, $p_0 = 0$ and $w = 1$. We generated 10^5 tumors with these parameters and stopped each simulation at the fixed time \tilde{t}_N defined by (7). At each cell division, the number of mutations acquired by each daughter cell was generated as a Poisson random variable with mean $w/2$. **(b)** The expected fixed-size spectrum (11) of Proposition 1 (solid red line) shows good agreement with the average spectrum of simulated tumors (grey dots) with the same parameters as in (a). We again generated 10^5 tumors with these parameters, but this time, we stopped each simulation when the tumor reached size N . The fundamental difference between the fixed-time and fixed-size spectrum is that the latter spectrum is restricted to $j = 1, \dots, N$, while the former spectrum has nonzero mass at values $j > N$.

as the (random) time at which the skeleton reaches size N . In Proposition 1 below, we provide the expected skeleton spectrum evaluated both at time \tilde{t}_N (fixed-time spectrum) and at time $\tilde{\tau}_N$ (fixed-size spectrum). Both the fixed-time and the fixed-size spectrum can be relevant to tumor data analysis depending on the context. For example, *in vitro* cell culture experiments and *in vivo* mouse experiments are often conducted over a fixed time period, in which case the fixed-time spectrum would apply. In the clinic, however, the size of a tumor is more readily measured than its age, in which case the fixed-size spectrum is more relevant [40]. It is therefore useful to understand both spectra and to what extent they differ.

Proposition 1. (1) Define \tilde{t}_N as in (7). Then, for any $N \geq 1$ and any $j \geq 1$,

$$\mathbb{E}[\tilde{S}_j(\tilde{t}_N)] = (w/q_0)N \cdot \int_0^{1-1/N} (1-y)y^{j-1} dy. \quad (9)$$

For any $j \geq 1$, then as $N \rightarrow \infty$,

$$\mathbb{E}[\tilde{S}_j(\tilde{t}_N)] \sim (w/q_0)N \cdot 1/(j(j+1)), \quad (10)$$

where $f(y) \sim g(y)$ as $y \rightarrow \infty$ means $\lim_{y \rightarrow \infty} f(y)/g(y) = 1$.

(2) Define $\tilde{\tau}_N$ as in (8). Then, for any $N \geq 2$,

$$\begin{aligned} & \mathbb{E}[\tilde{S}_j(\tilde{\tau}_N)] \\ &= \begin{cases} (w/q_0) \cdot \sum_{k=1}^{N-\max(2,j)} \frac{k}{N-j} \prod_{n=1}^{j-1} (1 - \frac{k}{N-n}) + w\delta_{1,j}, & 1 \leq j \leq N-1, \\ wp_0/q_0 = w/q_0 - w, & j = N, \end{cases} \end{aligned} \quad (11)$$

where $\prod_{\emptyset} := 1$ and $\delta_{\ell,m} = 1$ if $\ell = m$ and $\delta_{\ell,m} = 0$ otherwise.

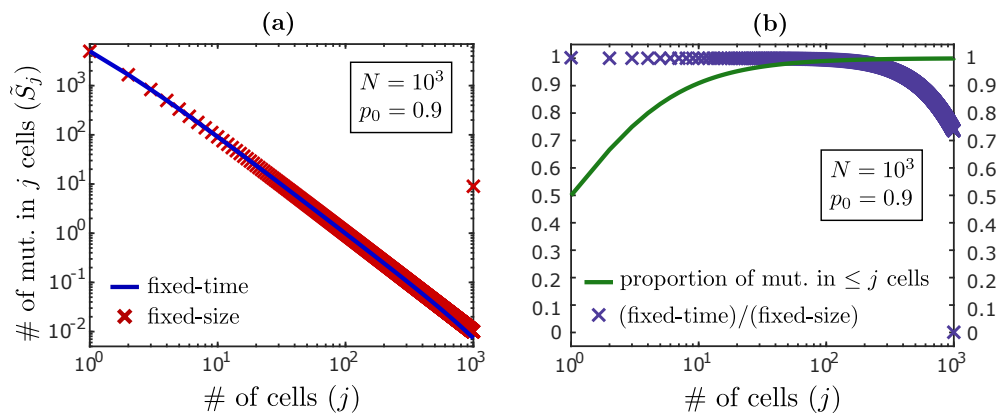


Figure 3: **(a)** The fixed-time spectrum (9) for the skeleton (blue curve) is a good approximation of the fixed-size spectrum (11) (red crosses) for mutations at frequencies $j \ll N$, given parameters $N = 10^3$, $p_0 = 0.9$ and $w = 1$. The two spectra diverge at larger frequencies, and the difference is substantial at $j = N$, since clonal mutations are concentrated at $j = N$ in the fixed-size spectrum, while they are scattered in the fixed-time spectrum. **(b)** Here, we show the ratio of the fixed-time spectrum to the fixed-size spectrum (purple crosses), and the proportion of mutations found in $\leq j$ skeleton cells (green curve). The fixed-time and fixed-size spectrum are virtually the same on $j \ll N$, where almost all mutations are found.

Proof. Appendix A. □

Analogous results for continuous mutation accumulation are presented in Appendix C. In Figure 2, we compare our fixed-time (9) and fixed-size (11) results with simulation results for $w = 1$, $p_0 = 0$ and $N = 100$. In this example, there are no clonal mutations, since $p_0 = 0$. The fundamental difference between the fixed-time and fixed-size spectrum is that the skeleton size at time \tilde{t}_N is variable, while it is always N at time $\tilde{\tau}_N$. The fixed-time spectrum therefore has nonzero mass at values $j > N$, due to instances in which the skeleton is larger than N at time \tilde{t}_N . It is however natural to ask how the fixed-time spectrum restricted to $j = 1, \dots, N$ relates to the fixed-size spectrum. To that end, note that for N large and $j \ll N$, the sum in (11) can be approximated by

$$(w/q_0) \cdot \sum_{k=1}^{N-\max(2,j)} \frac{k}{N-j} \prod_{n=1}^{j-1} \left(1 - \frac{k}{N-n}\right) \approx (w/q_0) \cdot \int_1^N \frac{k}{N} \left(1 - \frac{k}{N}\right)^{j-1} dk,$$

which, using the substitution $y := 1 - k/N$, becomes the fixed-time spectrum (9). In Figure 3a, we compare the two spectra for $p_0 = 0.9$ and $N = 10^3$, and show how the fixed-time spectrum is a good approximation of the fixed-size spectrum for $j \ll N$. In Figure 3b, we show that almost all mutations are found at $j \ll N$. In this example, the difference between the two spectra is within 1% on the range $j = 1, \dots, 150$, on which 99.3% of mutations are found. We finally note the sharp discontinuity at $j = N$ in the fixed-size spectrum of Figure 3a, which does not appear in the fixed-time spectrum. This is due to the distinct ways in which clonal mutations manifest in the two spectra. In the fixed-time spectrum, clonal mutations may appear at any value of j , depending on the skeleton size at time \tilde{t}_N . In the fixed-size spectrum, all these mutations are concentrated at $j = N$, which creates a large point mass at $j = N$.

3.3 Proportion of mutations found in one cell

We conclude this section by introducing two simple and important metrics derived from the site frequency spectrum of the skeleton. Note first that by (9) of Proposition 1, in the fixed-time spectrum, the expected number of mutations found in one skeleton cell is

$$\mathbb{E}[\tilde{S}_1(\tilde{t}_N)] = (1/2)(w/q_0)(N^2 - 1)/N \sim (1/2)(w/q_0)N, \quad N \rightarrow \infty. \quad (12)$$

Next, let $\tilde{M}_j(t) := \sum_{k \geq j} \tilde{S}_k(t)$ denote the number of mutations found in $\geq j$ skeleton cells at time t . Again, by (9) of Proposition 1, in the fixed-time spectrum, the expected total number of mutations on the skeleton is

$$\mathbb{E}[\tilde{M}_1(\tilde{t}_N)] = (w/q_0)(N - 1) \sim (w/q_0)N, \quad N \rightarrow \infty. \quad (13)$$

Expressions (12) and (13) suggest that for large N , half the mutations discovered at time \tilde{t}_N are found in only one cell. This is a consequence of the pure-birth exponential growth of the skeleton. Indeed, note that if we only consider the effective type-2 skeleton divisions, the total number of divisions required to reach generation k is $\sum_{j=0}^{k-1} 2^j = 2^k - 1$. The expected total number of mutations in generation k is then $(w/q_0)(2^k - 1)$, which is (13) with $N = 2^k$ as the number of cells in generation k . An additional 2^k divisions are required to reach generation $k + 1$, so each generation roughly doubles the total number of mutations. Of course, our model is stochastic, it operates in continuous time and generations may overlap, but this simple discrete argument gives intuition as to why half the mutations are found in one cell, and more generally why most mutations are found at the smallest frequencies.

4 Site frequency spectrum of total population and transition between power laws

When the extinction probability p_0 is small, i.e. tumor cell turnover is low, the SFS of the total population $(Z_0(t))_{t \geq 0}$ is well-approximated by the SFS of the skeleton $(\tilde{Z}_0(t))_{t \geq 0}$. However, tumor evolution is commonly characterized by high turnover, which induces a large mutational burden and high genetic diversity. For example, in [41], Avanzini & Antal estimate p_0 for metastatic breast cancer, colorectal cancer, head & neck cancer, lung cancer and prostate cancer as 0.90, 0.97, 0.95, 0.97 and 0.76, respectively. Bozic et al. [16] estimated p_0 as 0.93 for metastatic melanoma, and Bozic et al. [36] applied 0.72 for fast-growing colorectal cancer metastases and 0.99 for early tumor growth. Understanding how the SFS of these tumors behave, and exploring how they can potentially be identified from genomic data, is crucial due to their elevated genetic diversity and enhanced adaptability under treatment. To this end, we investigate in this section the expected fixed-time and fixed-size spectrum of the total population $(Z_0(t))_{t \geq 0}$. We show that as p_0 increases, the small-frequency end of the spectrum starts to deviate from the skeleton spectrum of Section 3, and as p_0 approaches 1, it transitions to the spectrum of a constant-sized population.

4.1 Expected fixed-time and fixed-size total population spectrum

Let $S_j(t)$ denote the number of mutations found in $j \geq 1$ cells at time t , the site frequency spectrum of the total cell population. We now wish to compute the mean of $S_j(t)$ conditioned on the tumor surviving to time t . We can compute the probability of this survival event as

$$\mathbb{P}(Z_0(t) > 0) = q_0 e^{\lambda_0 t} / (e^{\lambda_0 t} - p_0), \quad t \geq 0,$$

see (38) of Appendix B, and the expected size of a tumor that survives to time t as

$$\mathbb{E}[Z_0(t)|Z_0(t) > 0] = (e^{\lambda_0 t} - p_0)/q_0, \quad t \geq 0. \quad (14)$$

Note that $\mathbb{E}[Z_0(t)|Z_0(t) > 0] \sim e^{\lambda_0 t}/q_0$ as $t \rightarrow \infty$, which means that the long-run expected growth of a tumor conditioned on survival is exponential, where the exponential growth function has initial value $1/q_0$. Thus, while tumors with a small survival probability q_0 (large extinction probability p_0) are less likely to survive in the long run, those that do survive are larger on average than tumors with a large survival probability, since the latter tumors are less affected by the conditioning on survival. Now, for any integer $N \geq 1$, define

$$t_N := \log(q_0 N + p_0)/\lambda_0 \quad (15)$$

as the (fixed) time at which a surviving tumor has expected size N , and define

$$\tau_N := \inf\{t \geq 0 : Z_0(t) = N\} \quad (16)$$

as the (random) time at which the tumor reaches size N , with $\inf \emptyset = \infty$. In Proposition 2, we provide the expected SFS of $(Z_0(t))_{t \geq 0}$ at time t_N and τ_N , conditioned on the survival events $\{Z_0(t_N) > 0\}$ and $\{\tau_N < \infty\}$, respectively. In this case, we cannot obtain an explicit expression for the fixed-size spectrum, and provide instead a simple computational expression.

Proposition 2. (1) Define t_N as in (15). Then, for any $N \geq 1$ and $j \geq 1$,

$$\mathbb{E}[S_j(t_N)|Z_0(t_N) > 0] = wN \cdot \int_0^{1-1/N} (1 - p_0 y)^{-1} (1 - y) y^{j-1} dy. \quad (17)$$

For any $j \geq 1$, then as $N \rightarrow \infty$,

$$\begin{aligned} \mathbb{E}[S_j(t_N)|Z_0(t_N) > 0] &\sim wN \cdot \int_0^1 (1 - p_0 y)^{-1} (1 - y) y^{j-1} dy \\ &= wN \cdot \sum_{k=0}^{\infty} \frac{p_0^k}{(j+k)(j+k+1)}, \end{aligned} \quad (18)$$

where $f(y) \sim g(y)$ as $y \rightarrow \infty$ means $\lim_{y \rightarrow \infty} f(y)/g(y) = 1$.

(2) Define τ_N as in (16), let $\mathcal{S} := \{(\ell, m) : \ell, m \geq 0 \text{ and } \ell + m \leq N\}$ and $A := \{(0, 0)\} \cup \{(r, s) : r, s \geq 0 \text{ and } r + s = N\}$. Then, for any $N \geq 2$,

$$\mathbb{E}[S_j(\tau_N)|\tau_N < \infty] = (w/q_0) \cdot \sum_{k=1}^{N-1} (1 - p_0^{N-k}) \cdot h_{(1,k)}^{(j, N-j)}, \quad 1 \leq j \leq N, \quad (19)$$

where for $(r, s) \in A$, the vector $(h_{(\ell, m)}^{(r, s)})_{(\ell, m) \in \mathcal{S}}$ solves the system

$$\begin{aligned} &(\ell + m)(1 + p_0)h_{(\ell, m)}^{(r, s)} \\ &= \ell h_{(\ell+1, m)}^{(r, s)} + \ell p_0 h_{(\ell-1, m)}^{(r, s)} + m h_{(\ell, m+1)}^{(r, s)} + m p_0 h_{(\ell, m-1)}^{(r, s)}, \quad \ell, m \geq 1, \ell + m < N, \end{aligned}$$

with boundary conditions given by (46) in Appendix B.

Proof. Appendix B. □

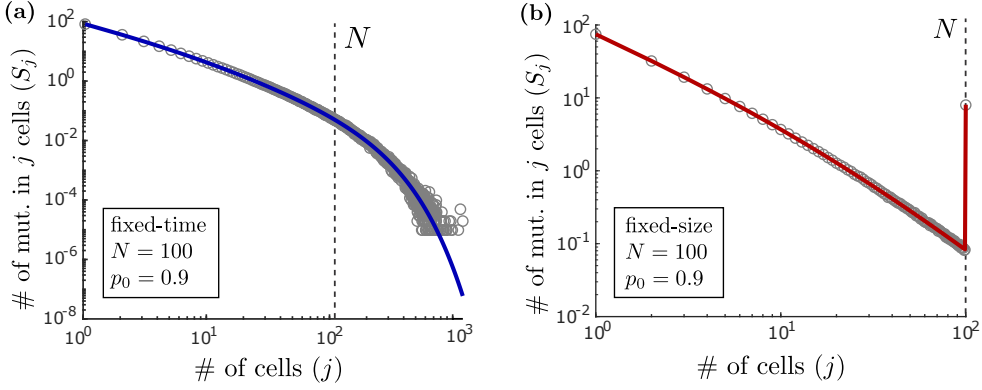


Figure 4: **(a)** The expected fixed-time spectrum (17) of Proposition 2 (solid blue line) shows good agreement with the average spectrum of simulated tumors (grey dots) for the parameters $N = 100$, $p_0 = 0.9$ and $w = 1$. We generated 10^5 tumors with these parameters and stopped each simulation at the fixed time t_N defined in (15). At each cell division, the number of mutations acquired by each daughter cell was generated as a Poisson random variable with mean $w/2$. **(b)** The expected fixed-size spectrum (19) of Proposition 2 (solid red line) shows good agreement with the average spectrum of simulated tumors (grey dots) with the same parameters as in (a). We again generated 10^5 tumors with these parameters, but this time, we stopped each simulation when the tumor reached size N . Note the discontinuity in the fixed-size spectrum at $j = N$, which is due to clonal mutations.

Analogous results for continuous mutation accumulation are presented in Appendix C. In Figure 4, we compare our fixed-time (17) and fixed-size (19) results with simulation results for $w = 1$, $p_0 = 0.9$ and $N = 100$. The fundamental difference between the two spectra is the same as we observed in Section 3.2. In Figure 5a, we compare them in more detail for $N = 100$ and $p_0 \in \{0, 0.5, 0.7, 0.9\}$. The fixed-time spectrum is a good approximation of the fixed-size spectrum on $j \ll N$ for all but $p_0 = 0.9$, in which case there is a significant difference even for $j \ll N$. In Figure 5b, we show that this difference reduces as N increases, with the expected number of mutations found in one cell being 1.46% off for $p = 0.9$ and $N = 1000$. The number of cells in 1 cm³ of tumor tissue is around $10^7 - 10^9$ [42], in which case the two spectra can be expected to agree on $j \ll N$ for most values of p_0 . They may diverge, however, when applied to smaller tumor tissue samples (1 mm³ or smaller) or tumor subclones, especially considering that the extinction probability can be as large as $p_0 = 0.99$.

The main reason that the two spectra behave similarly on $j \ll N$ for N sufficiently large is that once the tumor has reached a large size, its growth becomes essentially deterministic with exponential rate λ_0 . Mutations that arise late in the development of a large tumor therefore behave largely the same whether we stop at the fixed time t_N or the stochastic time τ_N . In fact, conditional on the nonextinction event Ω_∞ , $\tau_N/t_N \rightarrow 1$ in probability as $N \rightarrow \infty$, i.e. $\tau_N \approx t_N$ for large N [43]. As indicated by (14), tumor growth is not exponential initially, and the effect of the constant term p_0/q_0 increases as p_0 increases. Thus, the tumor enters its stable exponential growth phase later for larger values of p_0 , which is why two spectra can differ substantially for large values of p_0 when N is small. In Appendix D, we present a simple heuristic argument for why the two spectra agree on $j \ll N$, where we approximate the probabilities $h_{(1,k)}^{(j,N-j)}$ in (19) by continuous-time probabilities following [44].

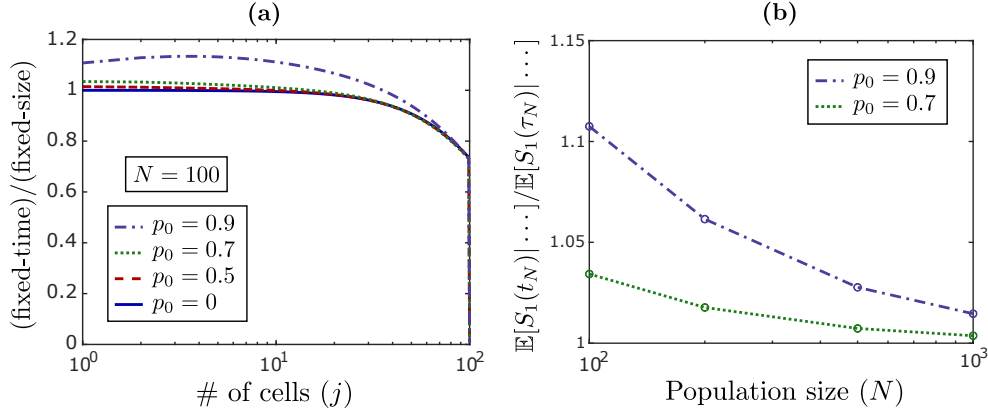


Figure 5: **(a)** Here, we show the ratio between the fixed-time spectrum (17) and the fixed-size spectrum (19) for $N = 100$, $p_0 \in \{0, 0.5, 0.7, 0.9\}$ and $w = 1$. The fixed-time spectrum is a good approximation of the fixed-size spectrum for smaller values of p_0 , but the two spectra start to diverge as p_0 increases. **(b)** Here, we show the ratio between the expected number of mutations found in one cell for the fixed-time spectrum and the fixed-size spectrum, as a function of the population size N , for $p_0 \in \{0.7, 0.9\}$ and $w = 1$. As N increases, the difference between the two spectra reduces both for $p_0 = 0.7$ and $p_0 = 0.9$.

4.2 Transition between power laws

By Proposition 1 of Section 3.2, the SFS of the skeleton depends on the mutation rate w and the extinction probability p_0 only through the effective mutation rate w/q_0 . By Proposition 2, however, the two parameters decouple in the SFS of the total population. The mutation rate w merely scales the total population spectrum by a linear factor, and the same is true for a large population size N , but the dependence on p_0 is more complicated. To better understand how p_0 affects the SFS, recall first that by (18), the asymptotic expected fixed-time spectrum is given by

$$\mathbb{E}[S_j(t_N) | Z_0(t_N) > 0] \sim wN \cdot \sum_{k=0}^{\infty} \frac{p_0^k}{(j+k)(j+k+1)}, \quad N \rightarrow \infty.$$

In Appendix E, we show that for fixed $0 < p_0 < 1$, sending $j \rightarrow \infty$ in this expression yields

$$wN \cdot \sum_{k=0}^{\infty} \frac{p_0^k}{(j+k)(j+k+1)} \sim (w/q_0)N \cdot 1/(j(j+1)), \quad j \rightarrow \infty, \quad (20)$$

which is the $1/j^2$ power law (10) of the asymptotic skeleton spectrum of Proposition 1. We also show that for fixed $j \geq 1$, sending $p_0 \rightarrow 1$ in the same expression yields

$$wN \cdot \sum_{k=0}^{\infty} \frac{p_0^k}{(j+k)(j+k+1)} \sim wN \cdot 1/j, \quad p_0 \rightarrow 1, \quad (21)$$

which is the $1/j$ power law of the constant-sized Moran model of population genetics, see e.g. Theorem 1.33 of [2]. When referring to results from [2], note that the population is assumed to have size $2N$, which is a common convention in population genetics.

Recall that when $p_0 = 0$, the spectrum of the total population $(Z_0(t))_{t \geq 0}$ is the spectrum of the skeleton $(\tilde{Z}_0(t))_{t \geq 0}$. Expressions (20) and (21) suggest that when $p_0 > 0$, the spectrum of $(Z_0(t))_{t \geq 0}$ continues to follow the $1/j^2$ skeleton law at the large-frequency end, while it starts to deviate from the $1/j^2$ law at the small-frequency end. In fact, as p_0 approaches 1, the small-frequency end transitions to the $1/j$ law of the constant-sized Moran model. This is illustrated in Figure 6 for $p_0 \in \{0.1, 0.5, 0.95\}$. Then, in Figure 7a, we show how for fixed

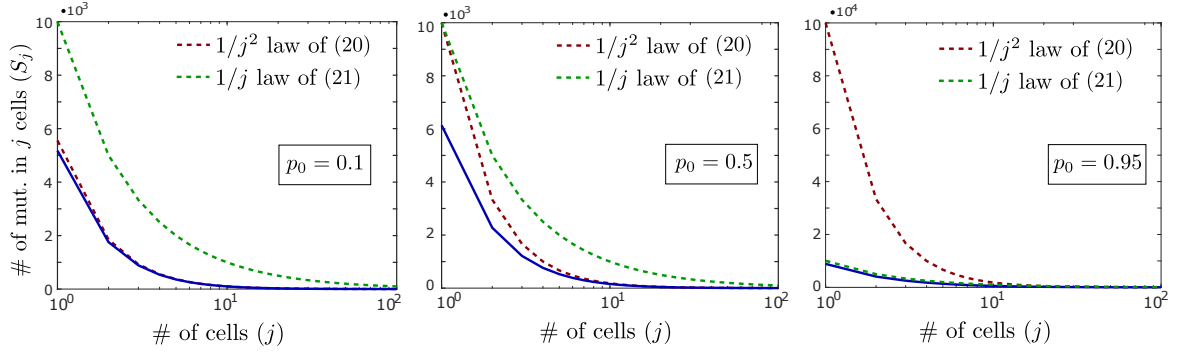


Figure 6: As the extinction probability p_0 is increased from $p_0 = 0.1$ to $p_0 = 0.95$, the small-frequency end of the asymptotic expected fixed-time spectrum (18) of Proposition 2 (solid blue line) transitions from the $1/j^2$ power law of (20) (dotted red line) to the $1/j$ power law of (21) (dotted green line). Other parameters are $N = 10^4$ and $w = 1$. Note that the $1/j$ law of (21) is fixed as a function of p_0 , while the $1/j^2$ law of (20) increases with p_0 .

$p_0 = 0.99$, the spectrum transitions from the $1/j^2$ law at the large-frequency end to the $1/j$ law at the small-frequency end. Note that the power laws of (20) and (21) intersect at

$$j = 1/q_0 - 1,$$

which gives an indication of the frequency at which the transition occurs. This intersecting point is independent of N , as is illustrated in Figure 7b (dotted vertical line).

To understand this transition between power laws, note that mutations that occur early in the evolution of a large tumor are only detected if they occur on the skeleton, which is why mutations at large frequencies follow the $1/j^2$ skeleton spectrum. For mutations that occur late, we need to consider both skeleton cells and finite-family cells. When p_0 is large, most cells are finite-family cells (their long-run proportion is p_0), and as p_0 approaches 1, finite-family clones start to behave like a critical branching process with net growth rate 0. This is why late mutations follow the $1/j$ law characteristic of a constant-sized population. Thus, even though the branching process dynamics of cell division and cell death are the same throughout the evolution of the tumor, from the perspective of mutation accumulation, the tumor effectively behaves like a pure-birth exponential growth process initially, and more like a constant-sized process at the end, assuming that the extinction probability p_0 is large. The transition between power laws is the transition between these two growth regimes.

4.3 Total mutational burden of the tumor

We next wish to quantify how p_0 affects overall mutation accumulation. To this end, we derive in Proposition 3 the expected total mutational burden of the tumor, both under the fixed-time and fixed-size spectrum. This quantity indicates the genetic diversity of the tumor, which has implications e.g. for its adaptability under treatment. It also enables us to compute a normalized version of the SFS, which is particularly useful for parameter estimation, as is discussed further in Sections 4.4 and 4.5 below. Before proceeding, define $M_j(t) := \sum_{k \geq j} S_k(t)$ as the number of mutations found in $\geq j$ cells at time t .

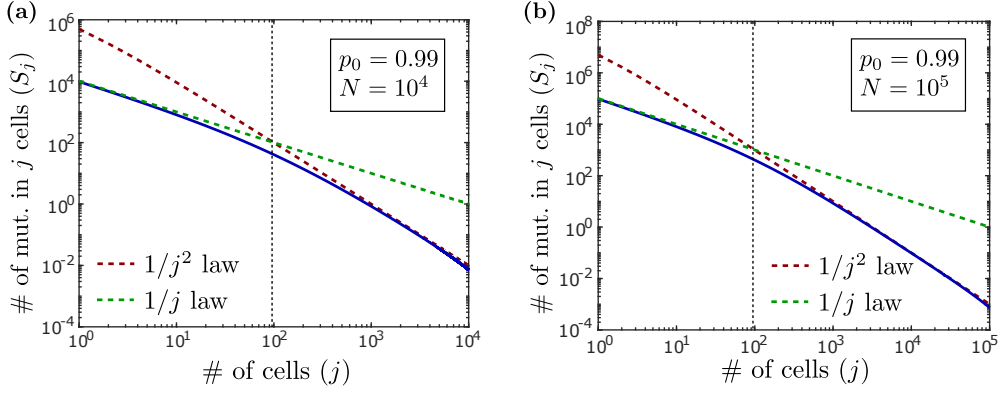


Figure 7: **(a)** For a fixed, large value of the extinction probability p_0 , the asymptotic expected fixed-time spectrum (18) of Proposition 2 (solid blue line) transitions from the $1/j^2$ power law of (20) (dotted red line) at the large-frequency end to the $1/j$ power law of (21) (dotted green line) at the small-frequency end. The parameters are $N = 10^4$, $p_0 = 0.99$ and $w = 1$. The dotted vertical line shows the intersecting point $j = 1/q_0 - 1$ of the two power laws in (20) and (21). **(b)** When we increase the tumor size to $N = 10^5$, the transition between power laws occurs around the same value of j as before, $j = 1/q_0 - 1$.

Proposition 3. (1) For $0 < p_0 < 1$, the expected total number of mutations in the fixed-time spectrum is given by

$$\begin{aligned} \mathbb{E}[M_1(t_N)|Z_0(t_N) > 0] &= -wN \cdot (1/p_0) \log(q_0 + p_0/N) \\ &\sim -wN \cdot \log(q_0)/p_0, \quad N \rightarrow \infty. \end{aligned} \quad (22)$$

For $p_0 = 0$, $\mathbb{E}[M_1(t_N)|Z_0(t_N) > 0] = w(N - 1) \sim wN$ as $N \rightarrow \infty$.

(2) Define \mathcal{S} and A as in Proposition 2. The expected total number of mutations in the fixed-size spectrum is given by

$$\mathbb{E}[M_1(\tau_N)|\tau_N < \infty] = (w/q_0) \cdot \sum_{k=1}^{N-1} (1 - p_0^{N-k}) (1 - h_{(1,k)}^{(0,N)} - h_{(1,k)}^{(0,0)}), \quad (23)$$

where for $(r, s) \in A$, the vector $(h_{(\ell,m)}^{(r,s)})_{(\ell,m) \in \mathcal{S}}$ solves the linear system in Proposition 2. For $p_0 = 0$, $\mathbb{E}[M_1(\tau_N)|\tau_N < \infty] = w(N - 1) \sim wN$ as $N \rightarrow \infty$.

Proof. Appendix F. □

For ease of notation, write $\overline{M}_1 := \mathbb{E}[M_1(t_N)|Z_0(t_N) > 0]$ as the expected total mutational burden under the fixed-time spectrum. We are interested in comparing \overline{M}_1 with the expected number of mutations under the $1/j^2$ skeleton law of (20). To this end, define

$$\widehat{M}_1 := (w/q_0)N, \quad (24)$$

following (13). This simple estimate has been used e.g. in [21], where they obtain a range of estimates of the total number of mutations in a hepatocellular carcinoma (HCC) tumor under different assumptions on tumor evolution. The ratio of \overline{M}_1 and \widehat{M}_1 is

$$\begin{aligned} \overline{M}_1/\widehat{M}_1 &= -(q_0/p_0) \cdot \log(q_0 + p_0/N) \\ &\sim -(q_0/p_0) \cdot \log(q_0), \quad N \rightarrow \infty. \end{aligned} \quad (25)$$

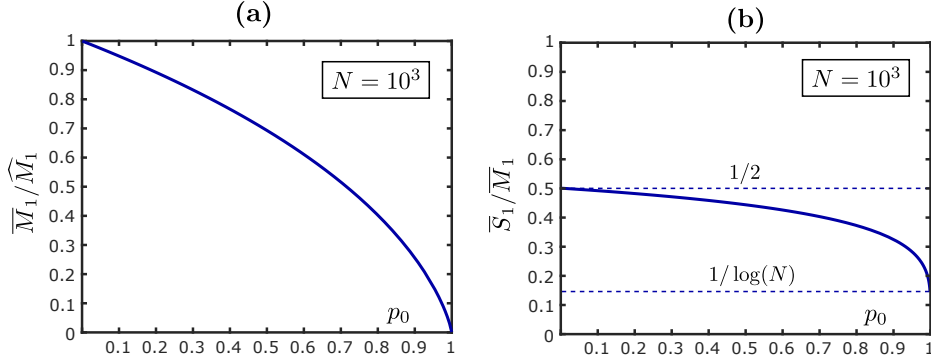


Figure 8: **(a)** Ratio between the expected number of mutations in the fixed-time spectrum, $\overline{M}_1 := \mathbb{E}[M_1(t_N)|Z_0(t_N) > 0]$ given by (22), and the simple estimate \widehat{M}_1 of (24), derived from the $1/j^2$ skeleton law of (20), as a function of p_0 for $N = 10^3$. The two estimates agree for $p_0 = 0$, but \widehat{M}_1 becomes a significant overestimate of \overline{M}_1 as p_0 increases. **(b)** The proportion of mutations found in one cell, $\overline{S}_1/\overline{M}_1 = \varphi_N(p_0)$ as given by (27), quantifies the transition between the $1/j^2$ and $1/j$ power laws at the small-frequency end of the spectrum. This transition accelerates as p_0 increases.

In Figure 8a, we show this ratio as a function of p_0 for $N = 1000$. The ratio is decreasing in p_0 , it converges to 1 as $p_0 \rightarrow 0$, and it converges to 0 as $p_0 \rightarrow 1$. To give some examples, in the $N \rightarrow \infty$ limit, $\overline{M}_1/\widehat{M}_1 = 0.46$ for $p_0 = 0.75$ and $\overline{M}_1/\widehat{M}_1 = 0.047$ for $p_0 = 0.99$. Thus, if one is interested in estimating the total number of mutations in an exponentially growing tumor, using the simple expression (24) implied by the skeleton spectrum will result in a significant overestimate when p_0 is large. Indeed, as p_0 increases, finite-family cells start to dominate the population, and they accumulate mutations less efficiently than skeleton cells.

4.4 Proportion of mutations found in one cell

At the extremes $p_0 = 0$ and $p_0 = 1$, the small-frequency end of the SFS is characterized by the $1/j^2$ skeleton law and the $1/j$ constant-sized law, respectively. To better understand how the small-frequency end behaves for intermediate values of p_0 , we next determine the relative proportion of mutations found at the very smallest frequency, i.e. in one cell. This metric quantifies the transition between the $1/j^2$ and $1/j$ power laws, and it enables us to propose a simple estimator for p_0 in Section 5 below. In Appendix G, we show that in the fixed-time spectrum, for $0 < p_0 < 1$, the expected number of mutations found in one cell is given by

$$\begin{aligned} \mathbb{E}[S_1(t_N)|Z_0(t_N) > 0] &= wN \cdot (1/p_0)(1 - 1/N + (q_0/p_0) \log(q_0 + p_0/N)) \\ &\sim wN \cdot (1/p_0)(1 + (q_0/p_0) \log(q_0)), \quad N \rightarrow \infty. \end{aligned} \quad (26)$$

As in Section 4.3, write $\overline{S}_1 := \mathbb{E}[S_1(t_N)|Z_0(t_N) > 0]$ for ease of notation. Then define $\varphi_N(p_0) := \overline{S}_1/\overline{M}_1$ as the proportion of mutations found in one cell. By (22) and (26),

$$\begin{aligned} \varphi_N(p_0) &= -(1 - 1/N + (q_0/p_0) \log(q_0 + p_0/N)) / \log(q_0 + p_0/N) \\ &\sim -(1 + (q_0/p_0) \log(q_0)) / \log(q_0), \quad N \rightarrow \infty. \end{aligned} \quad (27)$$

In Figure 8b, we show $\varphi_N = \overline{S}_1/\overline{M}_1$ as a function of p_0 for $N = 1000$. This function is strictly decreasing in p_0 , it converges to 0.50 as $p_0 \rightarrow 0$, and it converges to $(1 - 1/N)/\log(N)$ as $p_0 \rightarrow 1$, which is of order $1/\log(N)$ for N large. In the $p_0 \rightarrow 0$ regime, the SFS of the total

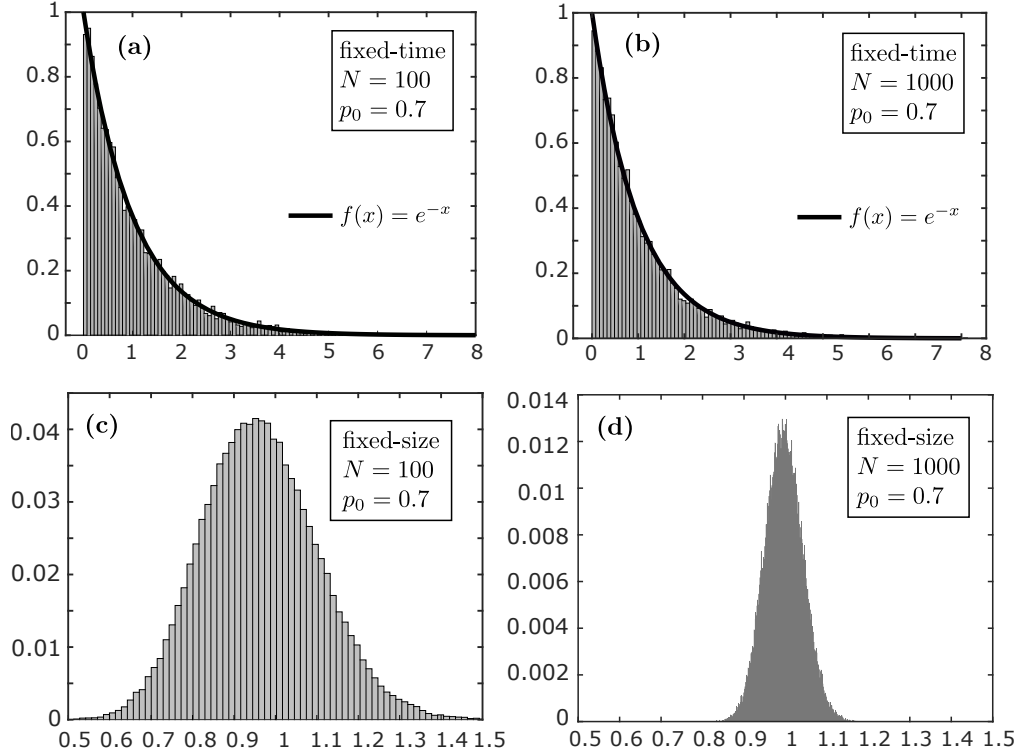


Figure 9: **(a)** Histogram of $S_1(t_N)/\bar{S}_1$ over 10^4 simulation runs with $N = 100$, $p = 0.7$ and $w = 1$, where t_N is defined by (15), and $\bar{S}_1 := \mathbb{E}[S_1(t_N)|Z_0(t_N) > 0]$ as given by (26). The y -axis is normalized so as to approximate the density of the underlying probability distribution. By comparison with the density $x \mapsto e^{-x}$, we see that $S_1(t_N)/\bar{S}_1$ is approximately a mean-1 exponential random variable, which is consistent with the law of large numbers (28). **(b)** When the population size is increased to $N = 1000$, $S_1(t_N)/\bar{S}_1$ retains the mean-1 exponential distribution, which is also consistent with (28). **(c)** Histogram of $S_1(\tau_N)/\bar{S}_1$ over 10^4 simulation runs with $N = 100$, $p = 0.7$ and $w = 1$, where τ_N is defined by (16). **(d)** Same as in (c), except now $N = 1000$. Together, (c) and (d) show that the ratio $S_1(\tau_N)/\bar{S}_1$ concentrates around 1 as N increases, which is consistent with the law of large numbers (29).

population $(Z_0(t))_{t \geq 0}$ is the SFS of the skeleton $(\tilde{Z}_0(t))_{t \geq 0}$, in which case half the mutations are found in one cell by Section 3.3. In the $p_0 \rightarrow 1$ regime, the SFS of $(Z_0(t))_{t \geq 0}$ is the SFS of the constant-sized Moran model, in which case the expected number of mutations is of order $wN \sum_{j=1}^N 1/j \sim wN \log(N)$ for N large, and the proportion of mutations found in one cell is of order $1/\log(N)$. Note that the rate of change $\varphi_N(p_0)$ increases as p_0 increases (Figure 8b). This means that the deviation from the $1/j^2$ skeleton law is initially slow for small values of p_0 , but it accelerates as p_0 increases and transitions quickly to the $1/j$ law for large values of p_0 . It also means that \bar{S}_1/\bar{M}_1 is more useful for distinguishing larger values of p_0 than smaller values, as will become more apparent in Section 5 below.

4.5 Spectra of individual large tumors (laws of large numbers)

The results of Proposition 2 hold in expectation, meaning that they apply to the average SFS computed over a large number of tumors. If we want to use these results to understand the evolutionary history of individual tumors, we need to know more about how well they apply

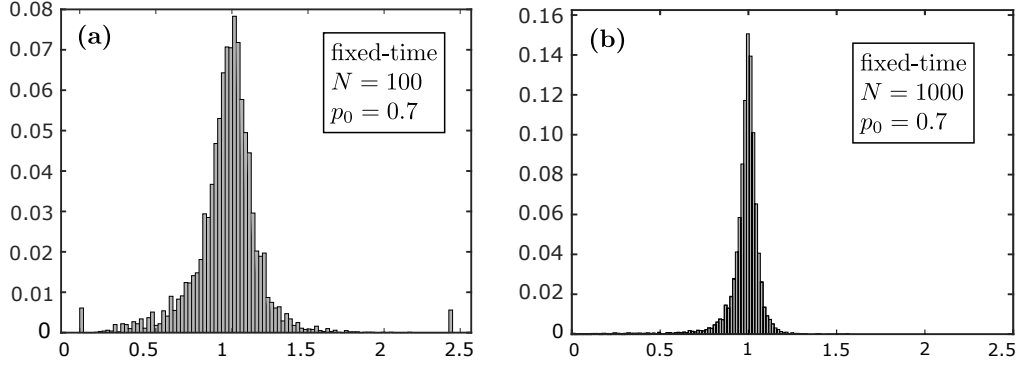


Figure 10: **(a)** Histogram of $(S_1(t_N)/M_1(t_N))/(\bar{S}_1/\bar{M}_1)$ over 10^4 simulation runs with $N = 100$, $p = 0.7$ and $w = 1$, where t_N is defined by (15), and the expected ratio \bar{S}_1/\bar{M}_1 is given by (27). Note the point masses at 0 and 2.44, which represent simulation runs where $S_1(t_N)/M_1(t_N) = 0$ and $S_1(t_N)/M_1(t_N) = 1$, respectively. **(b)** Same as in (a), except now, $N = 1000$. Together, (a) and (b) show that as N increases, $S_1(t_N)/M_1(t_N)$ concentrates around \bar{S}_1/\bar{M}_1 , which is consistent with the law of large numbers (28). It indicates that when the fixed-time spectrum is normalized by the number of mutations, it has the same deterministic law-of-large-numbers limit as the normalized fixed-size spectrum.

on a tumor-by-tumor basis. It is well-known that conditional on the nonextinction event Ω_∞ , $Z_0(t) \sim Y e^{\lambda_0 t}$ almost surely as $t \rightarrow \infty$, where Y follows the exponential distribution with mean $1/q_0$ (Theorem 1 of [33]). In words, the tumor population $Z_0(t)$ eventually grows at exponential rate λ_0 , but the initial value of the long-run exponential growth function is random and depends on the individual tumor. We can use this fact to formulate laws of large numbers for the fixed-time and fixed-size spectrum, which we state formally as a conjecture. In Appendix H, we present simple calculations in support of this result, and we also prove an analogous result (51) for a simplified, semideterministic version of our model.

Conjecture. (1) Define t_N as in (15). Then, there exists an exponential random variable X with mean 1 so that for any $j \geq 1$, conditional on Ω_∞ ,

$$S_j(t_N) \sim X \cdot wN \cdot \int_0^1 (1 - p_0 y)^{-1} (1 - y) y^{j-1} dy, \quad (28)$$

in probability or almost surely as $N \rightarrow \infty$.

(2) Define τ_N as in (16). Then, for any $j \geq 1$, conditional on Ω_∞ ,

$$S_j(\tau_N) \sim wN \cdot \int_0^1 (1 - p_0 y)^{-1} (1 - y) y^{j-1} dy, \quad (29)$$

in probability or almost surely as $N \rightarrow \infty$.

Both the fixed-time result (28) and the fixed-size result (29) agree with simulation results, see Figures 9 and 10. The difference between the two results is the random scaling factor X in (28), which reflects the fundamental difference between the fixed-time and fixed-size spectrum, i.e. that the tumor size is variable at time t_N , while it is always N at time τ_N . Note that since $\mathbb{E}[X] = 1$, the right-hand sides of (28) and (29) agree in the mean, and this mean agrees with the right-hand side of the asymptotic spectrum (18) of Proposition 2. Importantly, the scaling factor X in (28) is independent of j , so the proportion of mutations

found in j cells is the same in (18), (28) and (29). Thus, if we normalize the SFS with the total number of mutations, $S_j(t)/M_1(t)$, the fixed-time and fixed-size spectrum of an individual large tumor will be completely characterized by the asymptotic expected spectrum (18) of Proposition 2 (Figure 10). In particular, inference made from the normalized SFS of an individual large tumor is robust to whether it is observed at a fixed time or a fixed size. We will make use of this fact in our examination of a simple estimator for p_0 in Section 5.

5 Signatures of cell viability

In this section, we use our theoretical results to propose a simple estimator for the extinction probability p_0 , based on extracting one or more spatially separated subclones from a tumor, either clinically obtained or derived *in vitro* or *in vivo*. By a subclone, we mean all currently living descendants of a given common ancestor, i.e. all leaves of the branching tree started by a given tumor cell. We emphasize that since every clone or subclone derived from a single tumor cell obeys the same branching process dynamics as the overall tumor, all of our previous results can be applied to individual subclones.

Say that we sample a subclone of size n . For $1 \leq j \leq n-1$, let s_j be the number of mutations found in j cells of the subclone, and let $m_1 := \sum_{j=1}^{n-1} s_j$ be the total number of mutations. Here, we ignore mutations found in all cells of the subclone, since they include (i) mutations that accumulate prior to initiation of the tumor as a whole, (ii) mutations that occur post-tumor-initiation but prior to initiation of the subclone, and (iii) mutations that occur post-subclone-initiation but still end up in all subclone cells. Let \bar{s}_1 be the expected number of mutations in the subclone under the fixed-time spectrum, and let \bar{m}_1 be the expected total number of mutations under the fixed-time spectrum. By (27), we can write

$$\bar{s}_1/\bar{m}_1 = \varphi_n(p_0),$$

where $\varphi_n(p_0)$ is continuous and strictly decreasing in p_0 . In particular, $\varphi_n(p_0)$ is invertible. This implies that given \bar{s}_1 and \bar{m}_1 , p_0 can be recovered from this expression via

$$p_0 = \varphi_n^{-1}(\bar{s}_1/\bar{m}_1).$$

For the sampled values s_1 and m_1 , this suggests the following estimator for p_0 :

$$\hat{p}_0(n) := \varphi_n^{-1}(s_1/m_1). \quad (30)$$

Of course, if the subclone is sampled at a certain size, it makes more sense to use the fixed-size spectrum than the fixed-time spectrum. In addition, m_1 excludes mutations found in all cells of the subclone, while \bar{m}_1 includes some of these mutations. These potential sources of error are minor and can easily be resolved if necessary, as we discuss in more detail below. Note that the ratio of expected values \bar{s}_1/\bar{m}_1 takes values in $[(1-1/n)/\log(n), 1/2]$ by Section 4.4, whereas due to stochasticity, the sampled ratio s_1/m_1 can take any value in $[0, 1]$. To complete the estimator in (30), we therefore extend the definition of φ_n^{-1} by setting

$$\varphi_n^{-1}(x) := \begin{cases} 0, & 1/2 \leq x \leq 1, \\ 1, & 0 \leq x \leq (1-1/n)/\log(n). \end{cases} \quad (31)$$

For example, if we observe a ratio s_1/m_1 larger than $1/2$, we default to the estimate $\hat{p}_0(n) = 0$, since the expected ratio \bar{s}_1/\bar{m}_1 is largest (and equal to $1/2$) for $p_0 = 0$. Then, once p_0 has been estimated, an estimate for the mutation rate w can be obtained from (26) or (22).

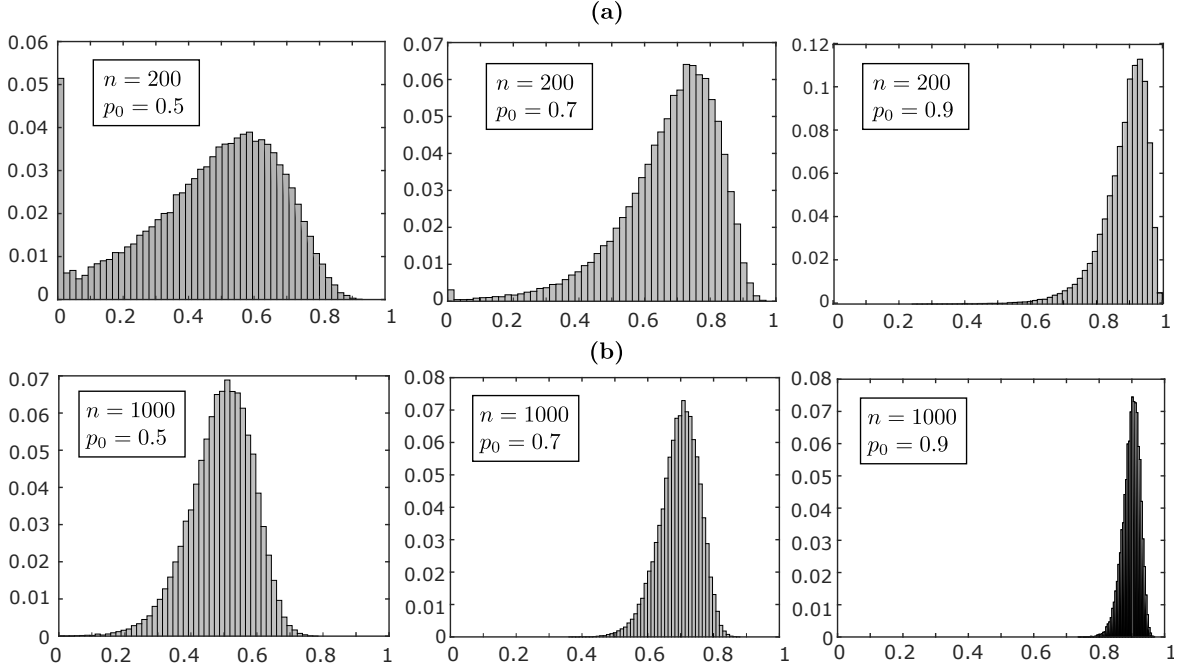


Figure 11: **(a)** Histogram of the estimator $\hat{p}_0(n)$ defined in (30) computed across 10^5 synthetic subclone samples of size $n = 200$, given true values $p_0 \in \{0.5, 0.7, 0.9\}$ and $w = 1$. **(b)** Same as in (a), except now $n = 1000$. Together, (a) and (b) show that as the size of the subclone is increased, the estimator $\hat{p}_0(n)$ concentrates around the true value of p_0 , which indicates statistical consistency of the estimator. They also show that the estimator gives the most accurate prediction of p_0 when p_0 is large.

The estimator $\hat{p}_0(n)$ has the benefit of being simple to define and to compute. However, as was mentioned above, it may make more sense to use the fixed-size spectrum than the fixed-time spectrum, and \bar{m}_1 includes clonal mutations that arise post-initiation of the subclone, whereas m_1 excludes these mutations. The second potential source of error is minor in most cases, and it can easily be removed simply by subtracting from \bar{m}_1 the contribution from mutations shared by all subclone cells. The first potential source of error is also insignificant when n is large, since we observed in Section 4.5 that the normalized spectrum of an individual large tumor or tumor subclone is robust to whether it is observed at a fixed time or a fixed size. For smaller values of n , one can replace \bar{s}_1 and \bar{m}_1 by the corresponding quantities (19) and (23) for the fixed-size spectrum, which we denote here by \bar{s}_1 and \bar{m}_1 . It remains true that we can write $\bar{s}_1/\bar{m}_1 = \psi_n(p_0)$ for some function ψ_n of p_0 , which allows us to define an estimator for p_0 as before. However, the fixed-size estimator has to be obtained numerically, e.g. by precomputing $\psi_n(p_0)$ over a grid of values of p_0 , and minimizing the error between the observed ratio s_1/m_1 and the expected ratio \bar{s}_1/\bar{m}_1 over the grid.

To further evaluate $\hat{p}_0(n)$, we use computer simulations to generate multiple independent subclones of size n with true extinction probability p_0 , and for each generated subclone, we compute the estimate $\hat{p}_0(n)$. In Figure 11a, we show a histogram for $\hat{p}_0(n)$ across 10^5 synthetic subclone samples of size $n = 200$ with true extinction probabilities $p_0 \in \{0.5, 0.7, 0.9\}$. In Table 1, we show performance metrics for $\hat{p}_0(n)$ computed across the 10^5 samples. For $p_0 = 0.5$, the estimator defaults to $\hat{p}_0(n) = 0$ for 4.6% of the subclone samples, for $p_0 = 0.7$,

n	p_0	mean	median	std. error	defaults to 0 (%)	defaults to 1 (%)
200	0.5	0.4694	0.5041	0.2099	0.0459	0
	0.7	0.6755	0.7045	0.1505	0.0026	0
	0.9	0.8839	0.9001	0.0725	0	0.00002
1000	0.5	0.4921	0.5000	0.0948	0.00002	0
	0.7	0.6957	0.7010	0.0603	0	0
	0.9	0.8979	0.9009	0.0266	0	0

Table 1: Performance metrics for the estimator $\hat{p}_0(n)$ computed from the data that underlies Figure 11. The standard error is the sample standard deviation from the mean. Both for $n = 200$ and $n = 1000$, the median estimate of $\hat{p}_0(n)$ accurately recovers the true value of p_0 , and the estimate improves in terms of standard error both as n increases and as p_0 increases.

it defaults to 0 in 0.3% of cases, and for $p_0 = 0.9$, it never defaults to 0. For all values of p_0 , the median estimate of $\hat{p}_0(n)$ accurately recovers the true value, and as p_0 increases, the quality of the estimate improves in terms of standard error (standard deviation from the mean). In Figure 11b, we increase the subclone size to $n = 1000$ and observe a marked improvement in the quality of $\hat{p}_0(n)$. This indicates statistical consistency of the estimator, meaning that $\hat{p}_0(n) \rightarrow p_0$ in probability as $n \rightarrow \infty$, which would also be a direct consequence of the law of large numbers (28) and the continuous mapping theorem. In words, the estimator recovers the true value of p_0 with arbitrarily high precision given a sufficiently large subclone. Note that the size of n required to return a high-precision estimate of $\hat{p}_0(n)$ becomes smaller as p_0 increases, making $\hat{p}_0(n)$ especially useful when p_0 is large. Indeed, as we remarked in Section 4.4, the rate of change of the expected ratio \bar{s}_1/\bar{m}_1 increases as p_0 increases, making it more useful for distinguishing between larger values of p_0 than smaller values.

Whenever it is possible to do multi-region sampling, there may be benefits from extracting multiple small, spatially separated subclones over a single large one. In this more general setting, we sample $K \geq 1$ subclones of size n . For $1 \leq j \leq n - 1$, let s_j^k be the number of mutations found in j cells of subclone number k , and let $m_1^k := \sum_{j=1}^{n-1} s_j^k$ be the total number of mutations in subclone k . We replace s_1 and m_1 in the definition of $\hat{p}_0(n)$ in (30) by the

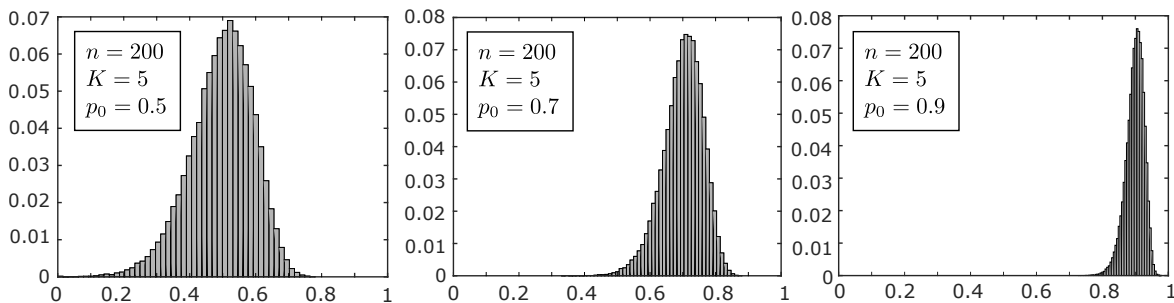


Figure 12: Histogram of the estimator $\hat{p}_0(n, K)$ of (32) computed across 10^5 synthetic samples of $K = 5$ subclones of size $n = 200$, given true values $p_0 \in \{0.5, 0.7, 0.9\}$ and $w = 1$. Note the similarity between these histograms and the histograms in (b) of Figure 11, which indicates that sampling five subclones of size 200 gives a comparable estimate of p_0 to sampling a single subclone of size 1000, using the estimator $\hat{p}_0(n, K)$ in both cases.

K	n	p_0	mean	median	std. error	defaults to 0 (%)	defaults to 1 (%)
5	200	0.5	0.4965	0.5050	0.0957	0.00013	0
		0.7	0.7000	0.7055	0.0612	0	0
		0.9	0.8983	0.9014	0.0279	0	0

Table 2: Performance metrics for the estimator $\hat{p}_0(n, K)$ computed from the data that underlies Figure 12. The standard error is the sample standard deviation from the mean. Note the similarity of these metrics with the lower half of Table 1.

sums $\sum_{k=1}^K s_1^k$ and $\sum_{k=1}^K m_1^k$ to obtain the estimator

$$\hat{p}_0(n, K) := \varphi_n^{-1} \left(\sum_{k=1}^K s_1^k / \sum_{k=1}^K m_1^k \right). \quad (32)$$

Of course, $\hat{p}_0(n, 1) = \hat{p}_0(n)$. In Figure 12, we show a histogram for $\hat{p}_0(n, K)$ evaluated across 10^5 synthetic samples, each sample consisting of $K = 5$ independent subclones of size $n = 200$. In Table 2, we show performance metrics computed across the 10^5 samples. Qualitatively, the histograms in Figure 12 are very similar to the histograms of Figure 11b, and quantitatively, the performance metrics in Table 2 mimic those for the $n = 1000$ case in Table 1. In other words, the quality of the estimate of p_0 obtained from sampling one subclone of size 1000 is comparable to the one obtained from sampling five subclones of size 200. In this scenario, it may make more sense to extract multiple small subclones than one large one, since it is impossible to tell from a single subclone sample alone whether the tumor as a whole can be considered as neutrally evolving. Should there be differences in the subclone dynamics, the multiregion sample will tease this out, and should the dynamics be the same, the estimate one obtains for p_0 will be of comparable quality to the single large subclone case.

6 Discussion

In this work, we have established exact expressions for the expected site frequency spectrum of a tumor, or more generally any population of individuals, that evolves according to a branching process with neutral mutations under the infinite-sites assumption of population genetics. We first considered the skeleton subpopulation, consisting of cells with an infinite line of descent, and obtained explicit expressions for SFS of the skeleton evaluated both at a fixed time and a fixed size. We then examined the total population, deriving an explicit expression for the fixed-time spectrum and a computational expression for the fixed-size spectrum. Our results apply to mutations at all frequencies, to tumor tissue samples and tumor subclones of any size, and to all values of the extinction probability p_0 , even values as large as $p_0 = 0.90$ and above, which are broadly relevant for cancer. Our work therefore offers a complete and rigorous characterization of the expected SFS of our branching process model of Section 2, and it contains results previously obtained in the literature as special or limiting cases, as we outline in detail in the next two paragraphs.

First, to compare our expected fixed-time and fixed-size skeleton spectrum, (9) and (11) of Proposition 1, to results previously obtained by Durrett [35, 33], Bozic et al. [36] and Williams et al. [22], note that for fixed $0 \leq f < 1$, the expected number of *subclonal* mutations found at frequency $\geq f$ in the population is, in the $N \rightarrow \infty$ limit,

$$\mathbb{E} \left[\sum_{j=\lceil Nf \rceil}^{N-1} \tilde{S}_j(\tilde{t}_N) \mid \Omega_\infty \right] \sim (w/q_0)N \cdot \sum_{j=\lceil Nf \rceil}^{N-1} 1/(j(j+1)) = (w/q_0)(1/f - 1). \quad (33)$$

This is the cumulative spectrum of subclonal mutations obtained in the above works. The result in Durrett [35, 33] is given for continuous mutation accumulation, and it includes clonal mutations, which by (47) of Appendix C requires adding $\nu/\lambda_0 = w/q_0$ mutations to (33). This yields $(\nu/\lambda_0)(1/f)$ as the cumulative spectrum, see Theorem 1 of [35] and Theorem 2 of [33]. Under discrete mutation accumulation, the number of clonal mutations is wp_0/q_0 by (11) of Proposition 1, yielding the cumulative spectrum $(w/q_0)(1/f) - w$ including clonal mutations. The difference of w reflects the difference in the number of clonal mutations between the discrete and continuous model, see Appendix C. Thus, our skeleton results, which hold for all values of p_0 and N , for discrete or continuous mutation accumulation, evaluated at a fixed time or a fixed size, contain the results of [35, 33, 36, 22] as asymptotic byproducts.

The expected fixed-time spectrum of the total population, (17) and (18) of Proposition 2, was previously obtained by Ohtsuki & Innan in [34], under the assumption of deterministic growth of the tumor bulk and stochastic growth of mutant subclones, which is a reasonable approximation when p_0 is small. We have established (17) and (18) for the fully stochastic model and for all values of p_0 by conditioning on tumor survival. We have also conjectured the laws of large numbers (28) and (29) for the fixed-time and fixed-size spectrum, which are supported by heuristic calculations and simulation results. We have proved a law of large numbers (51) for the semideterministic model of [34] in Appendix H, and we plan to prove the fully stochastic results (28) and (29) in a future work. The fixed-time law of large numbers has a stochastic limit, while the fixed-size limit is deterministic. However, if we normalize each spectrum by the total number of mutations, they converge to the same deterministic limit. This implies that analysis of the normalized spectrum of an individual large tumor is robust to whether it is observed at a fixed time or a fixed size. The fixed-size law of large numbers (29) agrees with Theorem 2.3 of Lambert [45], who considers a sample of individuals from a coalescent point process, a framework under which an infinite extant population is endowed with a coalescent structure that specifies how lineages coalesce when traced backwards in time. The expected fixed-size spectrum (19) of Proposition 2 is new as far as we know, as well as expressions (22) and (23) for the expected total mutational burden of Proposition 3.

All of the above results apply to the infinite-sites mutation model of population genetics. Cheek & Antal [46] have recently examined the SFS of an exponentially growing tumor without this assumption, citing single-cell sequencing results of Kuipers et al. [47] as motivation. They observe that if recurrent mutations are allowed, and there are S sites in the genome, the expected SFS at time t can be computed as $S\mathbb{P}(Y(t) = j)$, where $Y(t)$ is the number of mutants at time t in a two-type model of wild-type and mutant cells, each growing at the same rate. Then, to compute the SFS, one needs the distribution of $Y(t)$, which has been obtained under various simplifying assumptions, e.g. by Kessler & Levine [48] under the assumption of no cell death, and by Keller & Antal [49] under deterministic growth of the wild-types. Yet other authors have substituted the infinite-sites model with the *infinite-alleles* model, under which each new mutation creates a new type of individual, see e.g. [50, 51, 52]. Under this model, the site frequency spectrum is usually replaced by the *allele frequency spectrum*, which tracks frequencies of genetically distinct individuals, known as *haplotypes*.

Our complete theoretical results give rise to several important insights. First of all, whereas the fixed-time and fixed-size skeleton spectrum depends on the mutation rate w and the extinction probability p_0 only through the effective mutation rate w/q_0 , the two parameters decouple in the total population spectrum. The mutation rate w merely scales the spectrum linearly, whereas the extinction probability p_0 changes its shape at the small-frequency end. In fact, as p_0 increases from 0 to 1, the small-frequency end of the spectrum transitions from the $1/j^2$ power law characteristic of a pure-birth exponential growth to the

$1/j$ law characteristic of constant-sized populations. We examined the simple metrics $\overline{M}_1/\widehat{M}_1$ and $\overline{S}_1/\overline{M}_1$ that quantify this transition, where \widehat{M}_1 is the expected total mutational burden under the $1/j^2$ power law spectrum. We saw that $\overline{M}_1/\widehat{M}_1 \rightarrow 0$ as $p_0 \rightarrow 1$, which suggests that the simple estimate \widehat{M}_1 of the total number of mutations, applied e.g. in [21], is a significant overestimate of the actual number of mutations \overline{M}_1 when p_0 is large. We finally used the metric $\overline{S}_1/\overline{M}_1$ to propose a simple estimator for p_0 , based on sampling one or more spatially separated subclones from a tumor. This estimator accurately recovers the true value of p_0 from synthetic single-cell sequencing data, and it is most accurate when p_0 is large.

Our work reveals the information contained in the small-frequency end of the spectrum, on which most mutations are found. Accurately capturing mutations at small frequencies remains a technical challenge, even with the rapid advancement of single-cell sequencing technology. Current technology only reveals a small proportion of mutations in the tumor or tumor subclone, with large-frequency mutations most likely to be detected. Some of the above mentioned works have considered the site frequency spectrum of a small random sample of cells from a large tumor, see e.g. [35, 33, 34], and the more recent work [31] considers sampling DNA reads from the genomes of cells, which is a more relevant sampling scheme for current sequencing data. In a small random sample of cells, mutations shared by two or more cells in the sample are likely to have arisen early in tumor development, which means they will likely have occurred on the skeleton. As a result, the spectrum of a small random sample usually only contains information about the effective mutation rate w/q_0 . This fact has been used to estimate w/q_0 e.g. in [21, 22, 36] as mentioned in the introduction. Whether our proposed method of decoupling w and p_0 using the small-frequency end of the spectrum becomes tenable with higher-quality genomic data remains to be seen. In the meanwhile, it is likely necessary to go beyond the site frequency spectrum, which is indeed a crude summary statistic of the data, and use e.g. phylogenetic reconstruction to infer ancestral relationships, as in [37], and/or to complement genomic data gene expression data that can provide independent quantitative insights into the proliferation activity of extant cells.

Acknowledgements

EBG and KL were supported in part by NSF grant CMMI-1362236. EBG and JF were supported in part by NSF grant DMS-1349724.

Competing Interests

The authors declare no competing interests.

A Proof of Proposition 1

Proposition 1. (1) Define \tilde{t}_N as in (7). Then, for any $N \geq 1$ and any $j \geq 1$,

$$\mathbb{E}[\tilde{S}_j(\tilde{t}_N)] = (w/q_0)N \cdot \int_0^{1-1/N} (1-y)y^{j-1} dy.$$

For any $j \geq 1$, then as $N \rightarrow \infty$,

$$\mathbb{E}[\tilde{S}_j(\tilde{t}_N)] \sim (w/q_0)N \cdot 1/(j(j+1)),$$

where $f(y) \sim g(y)$ as $y \rightarrow \infty$ means $\lim_{y \rightarrow \infty} f(y)/g(y) = 1$.

(2) Define $\tilde{\tau}_N$ as in (8). Then, for any $N \geq 2$,

$$\mathbb{E}[\tilde{S}_j(\tilde{\tau}_N)] = \begin{cases} (w/q_0) \cdot \sum_{k=1}^{N-\max(2,j)} \frac{k}{N-j} \prod_{n=1}^{j-1} (1 - \frac{k}{N-n}) + w\delta_{1,j}, & 1 \leq j \leq N-1, \\ wp_0/q_0 = w/q_0 - w, & j = N, \end{cases}$$

where $\prod_{\emptyset} := 1$ and $\delta_{\ell,m} = 1$ if $\ell = m$ and $\delta_{\ell,m} = 0$ otherwise.

Proof. (1) By (3) in the main text, the mutation rate per skeleton cell per time unit is wr_0 . To stratify mutations based on their frequencies at time \tilde{t}_N , we define

$$\tilde{p}_j(s) := \mathbb{P}(\tilde{Z}_0(s) = j | \tilde{Z}_0(0) = 1), \quad j \geq 1, s \geq 0,$$

as the size-distribution at time s of a single-cell derived skeleton clone. Since $(\tilde{Z}_0(t))_{t \geq 0}$ is a Yule process with birth rate λ_0 , this distribution has an explicit expression,

$$\tilde{p}_j(s) = (1/e^{\lambda_0 s})(1 - 1/e^{\lambda_0 s})^{j-1}, \quad j \geq 1,$$

which is the geometric distribution with support $\{1, 2, \dots\}$ and success probability $1/e^{\lambda_0 s}$, see e.g. Section 3 of [33] (the support does not include 0 since skeleton clones do not go extinct). For $0 \leq t \leq \tilde{t}_N$, let $\tilde{S}_{j,\tilde{t}_N}(t)$ denote the number of mutations that accumulate in the time interval $[0, t]$ and are found in $j \geq 1$ skeleton cells at time \tilde{t}_N . We write $\tilde{S}_j(\tilde{t}_N) := \tilde{S}_{j,\tilde{t}_N}(\tilde{t}_N)$ for the site frequency spectrum of the skeleton at time \tilde{t}_N . If a mutation occurs during an infinitesimal time interval $[t, t + \Delta t]$, the clone started by the cell carrying the mutation has size j at time \tilde{t}_N with probability $\tilde{p}_j(\tilde{t}_N - t) + O(\Delta t)$, where $f(x) = O(x)$ means that there exists $C > 0$ so that $|f(x)| \leq Cx$ for sufficiently large x . The expected number of mutations that accumulate in $[t, t + \Delta t]$ and are present in $j \geq 1$ cells at time \tilde{t}_N is therefore

$$\mathbb{E}[\tilde{S}_{j,\tilde{t}_N}(t + \Delta t)] - \mathbb{E}[\tilde{S}_{j,\tilde{t}_N}(t)] = wr_0 e^{\lambda_0 t} \Delta t \cdot \tilde{p}_j(\tilde{t}_N - t) + o(\Delta t),$$

where we use that $\mathbb{E}[\tilde{Z}_0(t)] = e^{\lambda_0 t}$ is the mean skeleton size at time t , and $f(x) = o(x)$ means that $f(x)/x \rightarrow 0$ as $x \rightarrow 0$. A more precise mathematical argument for this statement is given in the proof of part (1) of Proposition 2 in Appendix B. Integrating over time, and using that $q_0 = \lambda_0/r_0$ by expression (1) and $N = e^{\lambda_0 \tilde{t}_N}$ by expression (7), we obtain

$$\begin{aligned} \mathbb{E}[\tilde{S}_j(\tilde{t}_N)] &= \int_0^{\tilde{t}_N} wr_0 \tilde{p}_j(\tilde{t}_N - t) e^{\lambda_0 t} dt \\ &= (w/q_0)N \cdot \int_0^{\tilde{t}_N} (e^{\lambda_0 t}/N)(1 - e^{\lambda_0 t}/N)^{j-1} \cdot \lambda_0 (e^{\lambda_0 t}/N) dt. \end{aligned}$$

Substituting $y = 1 - e^{\lambda_0 t}/N$, $dy = -\lambda_0 (e^{\lambda_0 t}/N) dt$, this implies

$$\mathbb{E}[\tilde{S}_j(\tilde{t}_N)] = (w/q_0)N \cdot \int_0^{1-1/N} (1-y)y^{j-1} dy, \quad (34)$$

the desired result. To obtain the asymptotic expression (10), it suffices to note that

$$\int_0^{1-1/N} (1-y)y^{j-1} dy = (1 - \frac{1}{N})^j \left(\frac{1}{j(j+1)} + \frac{1}{N} \frac{1}{j+1} \right).$$

(2) In (5) of Section 3.1, we showed that wp_0/q_0 mutations on average accumulate on type-1 divisions in between two type-2 divisions, while type-2 divisions add w mutations on average and change the skeleton level. Since the type-1 mutations on level $k = 1$ are

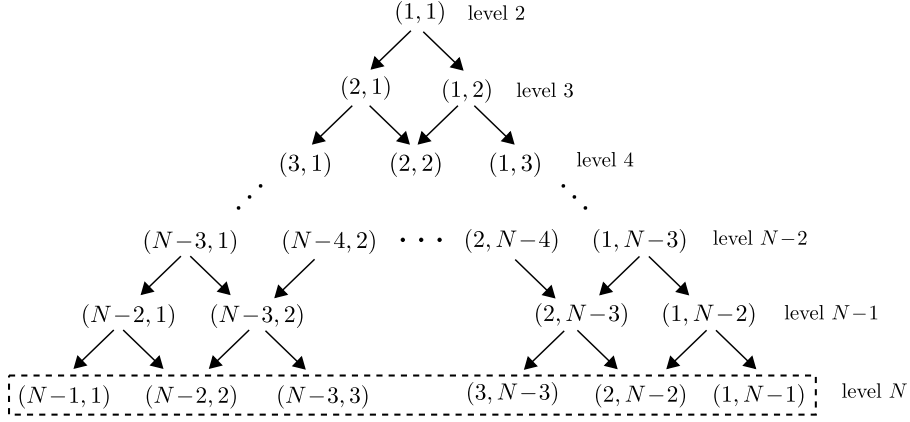


Figure 13: A diagram of the discrete-time Markov chain on $\{(\ell, m) : \ell, m \geq 1, \ell + m \leq N\}$ which tracks the number of mutated and non-mutated cells at each skeleton level. Each type-2 division increases the population level by one, and since skeleton cells do not die, the chain never returns to the lower levels. The states $(\ell, N - \ell)$ with $1 \leq \ell \leq N$ are absorbing (dashed box), since we are only interested in the evolution up until skeleton level N .

the clonal mutations, the expected number of clonal mutations is $w p_0 / q_0$, which is the $j = N$ case of the desired result. For $k = 2, \dots, N - 1$, however, the expected number of mutations on level k is $w p_0 / q_0 + w = w / q_0$, which includes the type-2 division that starts the level. For $1 \leq j \leq N - 1$, let $\tilde{h}_{(1, k-1)}^j$ be the probability that starting with one mutated and $k - 1$ non-mutated skeleton cells, there are j mutated cells when the skeleton reaches size N . Since for levels $k = 2, \dots, N - 1$, there are w / q_0 mutations on average per level, and each mutation on level k contributes $\tilde{h}_{(1, k-1)}^j$ to the expected number of mutations found in j cells at level N , we obtain

$$\mathbb{E}[\tilde{S}_j(\tilde{\tau}_N)] = (w/q_0) \sum_{k=2}^{N-1} \tilde{h}_{(1, k-1)}^j + w \delta_{1, j} = (w/q_0) \sum_{k=1}^{N-2} \tilde{h}_{(1, k)}^j + w \delta_{1, j}, \quad 1 \leq j \leq N - 1,$$

where the extra $w \delta_{1, j}$ term is due to mutations that occur on the final type-2 division that changes levels from $N - 1$ to N , each of which is found in one skeleton cell. The above informal argument is carried out in more mathematical detail in the proof of part (2) of Proposition 2 in Appendix B.

It remains to compute the probabilities $\tilde{h}_{(1, k)}^j$. To this end, define a two-dimensional discrete-time Markov chain on the state space $\{(\ell, m) : \ell, m \geq 1, \ell + m \leq N\}$, where the state (ℓ, m) keeps tracks of the number of mutants and non-mutants on population level $\ell + m$. Since each skeleton cell, mutated or non-mutated, divides into two cells at rate λ_0 , the transition probabilities for this chain are given by

$$\begin{aligned} (\ell, m) &\rightarrow (\ell + 1, m) && \text{w.p. } \ell / (\ell + m), \\ (\ell, m) &\rightarrow (\ell, m + 1) && \text{w.p. } m / (\ell + m), \end{aligned}$$

for $\ell, m \geq 1$ and $\ell + m < N$. The states $(\ell, N - \ell)$ for $1 \leq \ell \leq N - 1$ are absorbing. A diagram for this Markov chain is shown in Figure 13.

Let $\tilde{h}_{(\ell, m)}^r$ denote the probability that the above chain is absorbed at state $(r, N - r)$ when started from state (ℓ, m) . It is immediate that $\tilde{h}_{(\ell, m)}^r = 0$ if $\ell > r$ or $m > N - r$. For (ℓ, m) with $\ell \leq r$, $m \leq N - r$ and $\ell + m < N$, by conditioning on whether the

first transition out of state (ℓ, m) is to $(\ell + 1, m)$ or $(\ell, m + 1)$, we obtain the following recursion for $\tilde{h}_{(\ell, m)}^r$:

$$(\ell + m)\tilde{h}_{(\ell, m)}^r = \ell\tilde{h}_{(\ell+1, m)}^r + m\tilde{h}_{(\ell, m+1)}^r. \quad (35)$$

The boundary conditions are $\tilde{h}_{(\ell, N-\ell)}^r = \delta_{\ell, r}$ for $1 \leq \ell \leq N - 1$. We can actually compute $\tilde{h}_{(\ell, m)}^r$ directly as the sum of probabilities of all possible paths from (ℓ, m) to $(r, N - r)$, without using the above recursion. By noting that there are $\binom{N-(\ell+m)}{r-\ell}$ possible paths, and that each path has the same probability, we obtain

$$\tilde{h}_{(\ell, m)}^r = \binom{N-(\ell+m)}{r-\ell} \cdot \prod_{n=0}^{r-\ell-1} \frac{\ell+n}{\ell+m+n} \cdot \prod_{n=0}^{N-m-r-1} \frac{m+n}{r+m+n}, \quad (36)$$

with $\prod_{\emptyset} := 1$. As verification, it is straightforward to check that (36) solves (35).

To obtain $\tilde{h}_{(1, k)}^j$ for $1 \leq k \leq N - 2$ and $1 \leq j \leq N - 1$, note first that $\tilde{h}_{(1, k)}^j = 0$ for $k > N - j$. For $1 \leq k \leq \min(N - j, N - 2)$, we can simplify (36) to

$$\tilde{h}_{(1, k)}^j = \frac{k}{N-j} \cdot \prod_{n=1}^{j-1} \left(1 - \frac{k}{N-n}\right).$$

Thus, finally, for $1 \leq j \leq N - 1$,

$$\begin{aligned} \mathbb{E}[\tilde{S}_j(\tilde{\tau}_N)] &= (w/q_0) \sum_{k=1}^{N-2} \tilde{h}_{(1, k)}^j + w\delta_{1, j} \\ &= (w/q_0) \sum_{k=1}^{\min(N-j, N-2)} \frac{k}{N-j} \prod_{n=1}^{j-1} \left(1 - \frac{k}{N-n}\right) + w\delta_{1, j} \\ &= (w/q_0) \sum_{k=1}^{N-\max(2, j)} \frac{k}{N-j} \prod_{n=1}^{j-1} \left(1 - \frac{k}{N-n}\right) + w\delta_{1, j}. \end{aligned} \quad \square$$

B Proof of Proposition 2

Proposition 2. (1) Define t_N as in (15). Then, for any $N \geq 1$ and $j \geq 1$,

$$\mathbb{E}[S_j(t_N) | Z_0(t_N) > 0] = wN \cdot \int_0^{1-1/N} (1 - p_0 y)^{-1} (1 - y) y^{j-1} dy.$$

For any $j \geq 1$, then as $N \rightarrow \infty$,

$$\begin{aligned} \mathbb{E}[S_j(t_N) | Z_0(t_N) > 0] &\sim wN \cdot \int_0^1 (1 - p_0 y)^{-1} (1 - y) y^{j-1} dy \\ &= wN \cdot \sum_{k=0}^{\infty} \frac{p_0^k}{(j+k)(j+k+1)}, \end{aligned}$$

where $f(y) \sim g(y)$ as $y \rightarrow \infty$ means $\lim_{y \rightarrow \infty} f(y)/g(y) = 1$.

(2) Define τ_N as in (16), let $\mathcal{S} := \{(\ell, m) : \ell, m \geq 0 \text{ and } \ell + m \leq N\}$ and $A := \{(0, 0)\} \cup \{(r, s) : r, s \geq 0 \text{ and } r + s = N\}$. Then, for any $N \geq 2$,

$$\mathbb{E}[S_j(\tau_N) | \tau_N < \infty] = (w/q_0) \cdot \sum_{k=1}^{N-1} (1 - p_0^{N-k}) \cdot h_{(1, k)}^{(j, N-j)}, \quad 1 \leq j \leq N,$$

where for $(r, s) \in A$, the vector $(h_{(\ell, m)}^{(r, s)})_{(\ell, m) \in \mathcal{S}}$ solves the system

$$\begin{aligned} &(\ell + m)(1 + p_0)h_{(\ell, m)}^{(r, s)} \\ &= \ell h_{(\ell+1, m)}^{(r, s)} + \ell p_0 h_{(\ell-1, m)}^{(r, s)} + m h_{(\ell, m+1)}^{(r, s)} + m p_0 h_{(\ell, m-1)}^{(r, s)}, \quad \ell, m \geq 1, \ell + m < N, \end{aligned}$$

with boundary conditions given by (46) in Appendix B.

Proof. (1) We begin by defining

$$p_j(s) := \mathbb{P}(Z_0(s) = j | Z_0(0) = 1), \quad j \geq 0, s \geq 0,$$

as the size-distribution at time s of a single-cell derived clone. This distribution has an explicit expression: Setting

$$g(t) := \frac{p_0(e^{\lambda_0 t} - 1)}{e^{\lambda_0 t} - p_0} \quad \text{and} \quad h(t) := \frac{e^{\lambda_0 t} - 1}{e^{\lambda_0 t} - p_0},$$

we can write

$$\begin{aligned} p_0(t) &= \mathbb{P}(Z_0(t) = 0 | Z_0(0) = 1) = g(t), \\ p_j(t) &= \mathbb{P}(Z_0(t) = j | Z_0(0) = 1) = (1 - g(t))(1 - h(t))(h(t))^{j-1}, \quad j \geq 1, \end{aligned}$$

see e.g. (8) of [33]. Simplifying, we obtain

$$\begin{aligned} p_0(t) &= \frac{p_0(e^{\lambda_0 t} - 1)}{e^{\lambda_0 t} - p_0}, \\ p_j(t) &= \frac{q_0^2 e^{\lambda_0 t}}{(e^{\lambda_0 t} - p_0)^2} \cdot \left(\frac{e^{\lambda_0 t} - 1}{e^{\lambda_0 t} - p_0} \right)^{j-1}, \quad j \geq 1. \end{aligned} \tag{37}$$

The probability that a single-cell derived clone is still alive at time t is then given by

$$\mathbb{P}(Z_0(t) > 0 | Z_0(0) = 1) = 1 - p_0(t) = q_0 e^{\lambda_0 t} / (e^{\lambda_0 t} - p_0). \tag{38}$$

For $0 \leq t \leq t_N$, let $S_{j,t_N}(t)$ denote the number of mutations that accumulate in $[0, t]$ and are found in $j \geq 1$ cells at time t_N . We write $S_j(t_N) := S_{j,t_N}(t_N)$ for the site frequency spectrum at time t_N . Say a cell division occurs in an infinitesimal time interval $[t, t + \Delta t]$. The division results in w mutations on average, each assigned to one of the two daughter cells, and the clone started by this cell has size $j \geq 1$ cells at time t_N with probability $p_j(t_N - t) + O(\Delta t)$. We wish to show that on the event $\{Z_0(t_N) > 0\}$ of survival of the population up until time t_N , the expected number of mutations that accumulate in $[t, t + \Delta t]$ and are found in $j \geq 1$ cells at time t_N is

$$\mathbb{E}[(S_{j,t_N}(t + \Delta t) - S_{j,t_N}(t))1_{\{Z_0(t_N) > 0\}}] = wr_0 e^{\lambda_0 t} \Delta t \cdot p_j(t_N - t) + o(\Delta t), \tag{39}$$

where we use that $\mathbb{E}[Z_0(t)] = e^{\lambda_0 t}$. It will then follow from (39) that

$$\begin{aligned} &\mathbb{E}[S_{j,t_N}(t + \Delta t) - S_{j,t_N}(t) | Z_0(t_N) > 0] \\ &= wr_0 e^{\lambda_0 t} \Delta t \cdot p_j(t_N - t) / (1 - p_0(t_N)) + o(\Delta t). \end{aligned} \tag{40}$$

Note that the right-hand side of (39) is the number of mutations found in j cells at time t_N for the semideterministic model in which the tumor bulk grows deterministically at rate λ_0 , mutant clones arise at stochastic rate wr_0 , and mutant clones grow stochastically. It is not obvious that (39) should hold for the fully stochastic model, as including the event $\{Z_0(t_N) > 0\}$ of survival up until time t_N should presumably affect the population size at time $t \leq t_N$. The key is to observe that if a mutation occurs on a cell division at time t and ends up in $j \geq 1$ cells at time t_N , the population is automatically alive at time t_N . The relevant survival event in (39) is therefore $\{Z_0(t) > 0\}$, and the relevant population size factor is $\mathbb{E}[Z_0(t)1_{\{Z_0(t) > 0\}}] = \mathbb{E}[Z_0(t)] = e^{\lambda_0 t}$. To not distract further from the main calculations, we assume the reader is willing to accept (39) as true for the moment, and we provide a detailed mathematical argument at the end of the proof.

Using (40), we can integrate over time to obtain

$$\mathbb{E}[S_j(t_N)|Z_0(t_N) > 0] = (1 - p_0(t_N))^{-1} \cdot \int_0^{t_N} wr_0 e^{\lambda_0 t} p_j(t_N - t) dt. \quad (41)$$

Focusing on the integral, we write

$$\begin{aligned} & \int_0^{t_N} wr_0 e^{\lambda_0 t} p_j(t_N - t) dt \\ &= (w/q_0) \cdot \int_0^{t_N} \frac{q_0^2 e^{\lambda_0 t_N} e^{\lambda_0 t}}{(e^{\lambda_0 t_N} - p_0 e^{\lambda_0 t})^2} \cdot \left(\frac{e^{\lambda_0 t_N} - e^{\lambda_0 t}}{e^{\lambda_0 t_N} - p_0 e^{\lambda_0 t}} \right)^{j-1} \cdot \lambda_0 e^{\lambda_0 t} dt \\ &= wq_0 e^{\lambda_0 t_N} \cdot \int_0^{t_N} \frac{e^{\lambda_0 t}}{(e^{\lambda_0 t_N} - p_0 e^{\lambda_0 t})^2} \cdot \left(\frac{e^{\lambda_0 t_N} - e^{\lambda_0 t}}{e^{\lambda_0 t_N} - p_0 e^{\lambda_0 t}} \right)^{j-1} \cdot \lambda_0 e^{\lambda_0 t} dt. \end{aligned}$$

Set $L := e^{\lambda_0 t_N}$. Using the substitution $x := e^{\lambda_0 t}$, $dx = \lambda_0 e^{\lambda_0 t}$, we obtain

$$\int_0^{t_N} wr_0 e^{\lambda_0 t} p_j(t_N - t) dt = wq_0 L \cdot \int_1^L \frac{x}{(L - p_0 x)^2} \cdot \left(\frac{L - x}{L - p_0 x} \right)^{j-1} dx.$$

We again change variables, this time $y := (L - x)/(L - p_0 x)$, in which case

$$\begin{aligned} x &= L(1 - y)/(1 - p_0 y), \\ dx &= -q_0 L/(1 - p_0 y)^2 dy, \\ L - p_0 x &= q_0 L/(1 - p_0 y), \end{aligned}$$

and $y = (L - 1)/(L - p_0) = 1 - q_0/(L - p_0)$ for $x = 1$ and $y = 0$ for $x = L$, which implies

$$\int_0^{t_N} wr_0 e^{\lambda_0 t} p_j(t_N - t) dt = wL \cdot \int_0^{1 - q_0/(L - p_0)} (1 - p_0 y)^{-1} (1 - y) y^{j-1} dy. \quad (42)$$

We now apply (41) and (38) to see that

$$\mathbb{E}[S_j(t_N)|Z_0(t_N) > 0] = w \cdot \frac{e^{\lambda_0 t_N} - p_0}{q_0} \cdot \int_0^{1 - q_0/(e^{\lambda_0 t_N} - p_0)} (1 - p_0 y)^{-1} (1 - y) y^{j-1} dy,$$

and the desired result then follows from the fact that $(e^{\lambda_0 t_N} - p_0)/q_0 = N$ by the definition of t_N in (15).

To write the asymptotic expression (18) as a sum, note that

$$(1 - p_0 y)^{-1} = \sum_{k=0}^{\infty} p_0^k y^k,$$

which is valid for all $0 \leq p_0 < 1$ and $0 \leq y \leq 1$. It then follows that

$$\begin{aligned} \int_0^1 (1 - p_0 y)^{-1} (1 - y) y^{j-1} dy &= \sum_{k=0}^{\infty} p_0^k \left(\int_0^1 (1 - y) y^{j+k-1} dy \right) \\ &= \sum_{k=0}^{\infty} \frac{p_0^k}{(j+k)(j+k+1)}. \end{aligned}$$

We conclude by establishing (39) above, which was

$$\mathbb{E}[(S_{j,t_N}(t + \Delta t) - S_{j,t_N}(t))1_{\{Z_0(t_N) > 0\}}] = wr_0 e^{\lambda_0 t} \Delta t \cdot p_j(t_N - t) + o(\Delta t),$$

We decompose according to population size at time t . Assume that $Z_0(t) = k$ with $k \geq 1$, i.e. there are k cells at time t . Let $D_{t,\Delta t}$ denote the event that exactly one of the k cells divides in the infinitesimal time interval $[t, t + \Delta t]$, and enumerate the $k + 1$ cells after the cell division as Y_t^1, \dots, Y_t^{k+1} , where Y_t^1 and Y_t^2 are the two new cells. Let W denote the number of mutations that occur on the cell division, where W is a nonnegative integer-valued random variable with $\mathbb{E}[W] = w$, independent of $(Z_0(t))_{t \geq 0}$. For $\ell \geq 1$, let B_ℓ be

i.i.d. with $\mathbb{P}(B_\ell = 1) = \mathbb{P}(B_\ell = 2) = 1/2$, independent of $(Z_0(t))_{t \geq 0}$ and W , and assign mutation number ℓ to cell number B_ℓ for $1 \leq \ell \leq W$. Finally, let $Y_t^m(s)$ be the number of descendants of cell Y_t^m at time $t + s$ ($Y_t^m(0) = 1$). With this notation, define

$$A_{j,k,\ell}(t) := \{Z_0(t) = k\} \cap D_{t,\Delta t} \cap \{\ell \leq W\} \cap \{Y_t^{B_\ell}(t_N - t) = j\} \cap \{Z_0(t_N) > 0\}.$$

This is the event that the tumor survives to time t_N , that it consists of k cells at time t , that exactly one of the k cells divides in $[t, t + \Delta t]$, that at least ℓ mutations occur on this division, and that mutation number ℓ is found in j cells at time t_N . The reason we are interested in this event is that we can write

$$\mathbb{E}[(S_{j,t_N}(t + \Delta t) - S_{j,t_N}(t))1_{\{Z_0(t_N) > 0\}}] = \sum_{k=1}^{\infty} \sum_{\ell=1}^{\infty} \mathbb{P}(A_{j,k,\ell}(t)) + o(\Delta t),$$

where the $o(\Delta t)$ term captures the possibility of more than one cell division in $[t, t + \Delta t]$.

To compute $\mathbb{P}(A_{j,k,\ell}(t))$, note first that

$$\mathbb{P}(A_{j,k,\ell}(t)) = \mathbb{P}(\{Z_0(t) = k\} \cap D_{t,\Delta t} \cap \{\ell \leq W\} \cap \{Y_t^{B_\ell}(t_N - t) = j\}),$$

since the survival event $\{Z_0(t_N) > 0\}$ is implied by the other events. By independence,

$$\mathbb{P}(A_{j,k,\ell}(t)) = \mathbb{P}(\ell \leq W) \cdot \mathbb{P}(\{Z_0(t) = k\} \cap D_{t,\Delta t} \cap \{Y_t^{B_\ell}(t_N - t) = j\}),$$

To analyze the latter probability, note that since B_ℓ is independent of $(Z_0(t))_{t \geq 0}$, and $((Z_0(s))_{s \leq t}, (Y_t^1(s))_{s \geq 0}) = ((Z_0(s))_{s \leq t}, (Y_t^2(s))_{s \geq 0})$, we can write

$$\begin{aligned} & \mathbb{P}(\{Z_0(t) = k\} \cap D_{t,\Delta t} \cap \{Y_t^{B_\ell}(t_N - t) = j\}) \\ &= \mathbb{P}(\{Z_0(t) = k\} \cap D_{t,\Delta t} \cap \{Y_t^1(t_N - t) = j\}). \end{aligned}$$

Using the Markov property, we can calculate the latter probability as

$$\begin{aligned} & \mathbb{P}(\{Z_0(t) = k\} \cap D_{t,\Delta t} \cap \{Y_t^1(t_N - t) = j\}) \\ &= \mathbb{P}(Z_0(t) = k) \cdot \mathbb{P}(D_{t,\Delta t} | Z_0(t) = k) \cdot \mathbb{P}(Y_t^1(t_N - t) = j | Z_0(t) = k, D_{t,\Delta t}) \\ &= \mathbb{P}(Z_0(t) = k) \cdot e^{-kr_0\Delta t} kr_0\Delta t \cdot (p_j(t_N - t) + O(\Delta t)). \end{aligned}$$

Combining the above, we obtain

$$\begin{aligned} & \mathbb{E}[(S_{j,t_N}(t + \Delta t) - S_{j,t_N}(t))1_{\{Z_0(t_N) > 0\}}] \\ &= \sum_{k=1}^{\infty} \sum_{\ell=1}^{\infty} \mathbb{P}(A_{j,k,\ell}(t)) + o(\Delta t) \\ &= r_0 p_j(t_N - t) \Delta t \cdot \left(\sum_{\ell=1}^{\infty} \mathbb{P}(W \geq \ell) \right) \cdot \left(\sum_{k=1}^{\infty} k \mathbb{P}(Z_0(t) = k) \right) + o(\Delta t) \\ &= wr_0 e^{\lambda_0 t} \Delta t \cdot p_j(t_N - t) + o(\Delta t), \end{aligned}$$

where we use $\sum_{\ell=1}^{\infty} \mathbb{P}(W \geq \ell) = \mathbb{E}[W] = w$ and $\sum_{k=1}^{\infty} k \mathbb{P}(Z_0(t) = k) = \mathbb{E}[Z_0(t)] = e^{\lambda_0 t}$. This concludes the proof.

- (2) Let $(X_n)_{n \geq 0}$ denote the discrete-time jump process embedded in $(Z_0(t))_{t \geq 0}$ that only keeps track of changes in population size. More precisely, if σ_n is the time of the n -th jump of $(Z_0(t))_{t \geq 0}$, $n \geq 1$, then $X_0 = 1$ and $X_n = Z_0(\sigma_n)$ for $n \geq 1$. Since cells divide at rate r_0 and die at rate d_0 , $(X_n)_{n \geq 0}$ is a simple random walk, absorbed at 0, which moves up with probability $a := r_0/(r_0 + d_0) = 1/(1 + p_0)$ and down with

probability $b = 1 - a = p_0/(1 + p_0)$. Since we are only interested in what happens until the population either goes extinct or reaches level N , we treat N as an absorbing state. Define

$$T_k := \inf\{n \geq 0 : X_n = k\}, \quad 0 \leq k \leq N, \quad (43)$$

as the (discrete) time at which the random walk first hits level k , with $\inf \emptyset = \infty$. Let \mathbb{P}_j denote the probability measure of $(X_n)_{n \geq 0}$ when started at $X_0 = j$. By the gambler's ruin formula,

$$\mathbb{P}_j(T_k < T_0) = (1 - p_0^j)/(1 - p_0^k), \quad 0 \leq j \leq k. \quad (44)$$

For $1 \leq k \leq N - 1$, let $\Lambda_{k,k+1}$ denote the number of transitions from k to $k + 1$,

$$\Lambda_{k,k+1} := \sum_{j=0}^{\infty} \mathbf{1}_{\{Z_j=k, Z_{j+1}=k+1\}}.$$

and let Λ_k denote the number of visits to k ,

$$\Lambda_k := \sum_{j=0}^{\infty} \mathbf{1}_{\{Z_j=k\}}.$$

By the strong Markov property and (44), we can write

$$\mathbb{E}_1[\Lambda_k] = \mathbb{P}_1(T_k < T_0) \cdot \mathbb{E}_k[\Lambda_k] = \frac{q_0}{1-p_0^k} \cdot \mathbb{E}_k[\Lambda_k].$$

When the chain leaves state k , it moves up with probability $1/(1 + p_0)$ and down with probability $p_0/(1 + p_0)$. Starting from $k + 1$, the probability that the chain does not return to k (probability it is absorbed at N) is $q_0/(1 - p_0^{N-k})$ by (44), and starting from $k - 1$, the probability it does not return to k (probability it is absorbed at 0) is $1 - (1 - p_0^{k-1})/(1 - p_0^k)$ again by (44). Thus, starting from k , Λ_k has the geometric distribution with support $\{1, 2, \dots\}$ and success probability

$$\frac{1}{1+p_0} \cdot \frac{q_0}{1-p_0^{N-k}} + \frac{p_0}{1+p_0} \cdot \left(1 - \frac{1-p_0^{k-1}}{1-p_0^k}\right) = \frac{q_0(1-p_0^N)}{(1+p_0)(1-p_0^k)(1-p_0^{N-k})}.$$

It follows that

$$\begin{aligned} \mathbb{E}_1[\Lambda_k] &= \frac{(1+p_0)(1-p_0^{N-k})}{1-p_0^N}, \\ \mathbb{E}_1[\Lambda_{k,k+1}] &= \frac{1}{1+p_0} \cdot \mathbb{E}_1[\Lambda_k] = \frac{1-p_0^{N-k}}{1-p_0^N}. \end{aligned} \quad (45)$$

For $1 \leq k \leq N - 1$, define $T_{k,k+1}^i$ as the (discrete) time of the i -th transition from k to $k + 1$,

$$T_{k,k+1}^i := \inf\{n > T_{k,k+1}^{i-1} : X_{n-1} = k, X_n = k + 1\}, \quad i \geq 1,$$

with $T_{k,k+1}^0 := 0$ and $\inf \emptyset = \infty$. A transition from k to $k + 1$ in $(X_n)_{n \geq 0}$ occurs due to one of the k cells in the original process $(Z_0(t))_{t \geq 0}$ dividing. Assume $W_{i,k}$ mutations occur on the i -th such transition, where $W_{i,k}$ are i.i.d. nonnegative integer-valued random variables with $\mathbb{E}[W_{i,k}] = w$, independent of $(X_n)_{n \geq 0}$. Enumerate the cells at time $T_{k,k+1}^i$ as $Y_{i,k}^1, \dots, Y_{i,k}^{k+1}$. By the same argument as laid out in part (1) above, we can assume that each mutation is assigned to the first cell. Let $Y_{i,k}^m(n)$ be the number of descendants of cell $Y_{i,k}^m$ at time step $T_{k,k+1}^i + n$ ($Y_{i,k}^m(0) = 1$). Then define the event

$$A_{j,k,i,\ell} := \{T_N < T_0, T_{k,k+1}^i < \infty, \ell \leq W_{i,k}, Y_{i,k}^1(T_N - T_{k,k+1}^i) = j\}.$$

This is the event that the random walk eventually hits level N , that it transitions at least i times from k to $k + 1$ before doing so, that at least ℓ mutations occur on the i -th such transition, and that the ℓ -th mutation is found in j cells at level N . We can then write

$$\begin{aligned}\mathbb{E}[S_j(\tau_N)|\tau_N < \infty] &= (\mathbb{P}_1(T_N < T_0))^{-1} \cdot \sum_{k=1}^{N-1} \sum_{i=1}^{\infty} \sum_{\ell=1}^{\infty} \mathbb{P}_1(A_{j,k,i,\ell}) \\ &= \frac{1-p_0^N}{q_0} \cdot \sum_{k=1}^{N-1} \sum_{i=1}^{\infty} \sum_{\ell=1}^{\infty} \mathbb{P}_1(A_{j,k,i,\ell}).\end{aligned}$$

To compute $\mathbb{P}_1(A_{j,k,i,\ell})$, note first that by independence,

$$\begin{aligned}\mathbb{P}_1(T_N < T_0, T_{k,k+1}^i < \infty, \ell \leq W_{i,k}, Y_{i,k}^1(T_N - T_{k,k+1}^i) = j) \\ = \mathbb{P}(\ell \leq W_{i,k}) \cdot \mathbb{P}_1(T_N < T_0, T_{k,k+1}^i < \infty, Y_{i,k}^1(T_N - T_{k,k+1}^i) = j).\end{aligned}$$

By the strong Markov property, with $j \geq 1$,

$$\begin{aligned}\mathbb{P}_1(T_N < T_0, T_{k,k+1}^i < \infty, Y_{i,k}^1(T_N - T_{k,k+1}^i) = j) \\ = \mathbb{P}_1(T_N < T_0, Y_{i,k}^1(T_N - T_{k,k+1}^i) = j | T_{k,k+1}^i < \infty) \cdot \mathbb{P}(T_{k,k+1}^i < \infty) \\ = \mathbb{P}_{k+1}(T_N < T_0, Y^1(T_N) = j) \cdot \mathbb{P}_1(T_{k,k+1}^i < \infty),\end{aligned}$$

where we restart the chain at the stopping time $T_{k,k+1}^i$ with $k + 1$ cells enumerated as Y^1, \dots, Y^{k+1} . Define $h_{(1,k)}^{(j,N-j)} := \mathbb{P}_{k+1}(T_N < T_0, Y^1(T_N) = j)$ for the moment, i.e. the probability that starting with 1 mutated and k non-mutated cells, there are j mutated and $N - j$ non-mutated cells when the population reaches level N . We can then write

$$\begin{aligned}\mathbb{P}_1(T_N < T_0, T_{k,k+1}^i < \infty, Y_{i,k}^1(T_N - T_{k,k+1}^i) = j) \\ = h_{(1,k)}^{(j,N-j)} \cdot \mathbb{P}_1(T_{k,k+1}^i < \infty).\end{aligned}$$

Combining the above, and using $\mathbb{E}_1[\Lambda_{k,k+1}] = (1 - p_0^{N-k})/(1 - p_0^N)$ by (45), we obtain

$$\begin{aligned}\mathbb{E}[S_j(\tau_N)|\tau_N < \infty] \\ = \frac{1-p_0^N}{q_0} \cdot \sum_{k=1}^{N-1} \left(\sum_{i=1}^{\infty} \left(\sum_{\ell=1}^{\infty} \mathbb{P}(W_{i,k} \geq \ell) \right) \cdot \mathbb{P}_1(T_{k,k+1}^i < \infty) \right) \cdot h_{(1,k)}^{(j,N-j)} \\ = \frac{1-p_0^N}{q_0} \cdot \sum_{k=1}^{N-1} w \cdot \mathbb{E}_1[\Lambda_{k,k+1}] \cdot h_{(1,k)}^{(j,N-j)} \\ = (w/q_0) \cdot \sum_{k=1}^{N-1} (1 - p_0^{N-k}) h_{(1,k)}^{(j,N-j)},\end{aligned}$$

which is the desired result.

It remains to show how the probabilities $h_{(1,k)}^{(j,N-j)}$ for $1 \leq j \leq N$ can be computed. As in the proof of (1) of Proposition 1, one can observe that $h_{(\ell,m)}^{(r,N-r)}$ is the probability of absorption in state $(r, N - r)$, starting from state (ℓ, m) , for a Markov chain on state space $\mathcal{S} := \{(\ell, m) : \ell, m \geq 0 \text{ and } \ell + m \leq N\}$, where the state (ℓ, m) keeps track of the number of mutated and non-mutated cells at population level $\ell + m$. The difference is that now, cells can die, so population level changes can both be up and down. The transition probabilities are therefore more complex in this case, and given by

$$\begin{aligned}(\ell, m) \rightarrow (\ell + 1, m) & \text{ w.p. } \ell r_0 / ((\ell + m)(r_0 + d_0)) = \ell / ((\ell + m)(1 + p_0)), \\ (\ell, m) \rightarrow (\ell - 1, m) & \text{ w.p. } \ell d_0 / ((\ell + m)(r_0 + d_0)) = \ell p_0 / ((\ell + m)(1 + p_0)), \\ (\ell, m) \rightarrow (\ell, m + 1) & \text{ w.p. } m r_0 / ((\ell + m)(r_0 + d_0)) = m / ((\ell + m)(1 + p_0)), \\ (\ell, m) \rightarrow (\ell, m - 1) & \text{ w.p. } m d_0 / ((\ell + m)(r_0 + d_0)) = m p_0 / ((\ell + m)(1 + p_0)),\end{aligned}$$

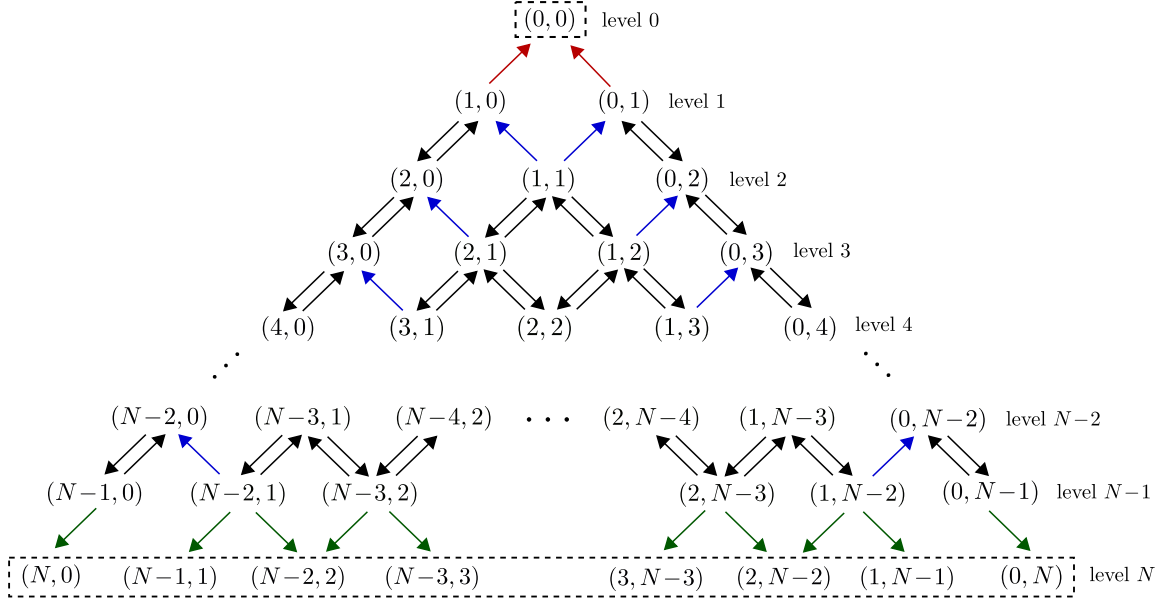


Figure 14: A diagram of the discrete-time Markov chain on $\mathcal{S} := \{(\ell, m) : \ell, m \geq 0, \ell + m \leq N\}$ that tracks the number of mutated and non-mutated cells at each population level. Contrary to the chain for the skeleton process of Proposition 1 (Figure 13), we now incorporate cell death, which means both that population level changes can be up and down, and that we add states of the form (ℓ, m) with $\ell = 0$ or $m = 0$. The states $(0, 0)$ and $\{(\ell, N - \ell)\}_{0 \leq \ell \leq N}$ are absorbing, and the states $\{(\ell, m) : \ell, m \geq 1, \ell + m < N\}$, $\{(\ell, 0)\}_{1 \leq \ell \leq N-1}$ and $\{(0, m)\}_{1 \leq m \leq N-1}$ form their respective communicating classes. Colored arrows indicate transitions out of communicating classes and dashed boxes identify absorbing states.

for (ℓ, m) with $\ell, m \geq 0$ and $0 < \ell + m < N$. The states $(0, 0)$ and $(\ell, N - \ell)$ with $0 \leq \ell \leq N$ are absorbing. A diagram of the Markov chain is shown in Figure 14.

For given $(r, s) \in A := \{(0, 0)\} \cup \{(r, s) : r, s \geq 0 \text{ and } r + s = N\}$ and (ℓ, m) with $\ell, m \geq 0$ and $0 < \ell + m < N$, by conditioning on the first transition out of state (ℓ, m) , we can derive the following recursion for $h_{(\ell, m)}^{(r, s)}$:

$$(\ell + m)(1 + p_0)h_{(\ell, m)}^{(r, s)} = \ell h_{(\ell+1, m)}^{(r, s)} + \ell p_0 h_{(\ell-1, m)}^{(r, s)} + m h_{(\ell, m+1)}^{(r, s)} + m p_0 h_{(\ell, m-1)}^{(r, s)}.$$

By the gambler's ruin formula (44), the boundary conditions are

$$\begin{aligned} h_{(\ell, 0)}^{(N, 0)} &= 1 - h_{(\ell, 0)}^{(0, 0)} = (1 - p_0^\ell)/(1 - p_0^N), \quad 0 \leq \ell \leq N, \\ h_{(\ell, 0)}^{(r, s)} &= 0, \quad 0 \leq \ell \leq N, \quad (r, s) \notin \{(0, 0), (N, 0)\} \\ h_{(0, m)}^{(0, N)} &= 1 - h_{(0, m)}^{(0, 0)} = (1 - p_0^m)/(1 - p_0^N), \quad 0 \leq m \leq N, \\ h_{(0, m)}^{(r, s)} &= 0, \quad 0 \leq m \leq N, \quad (r, s) \notin \{(0, 0), (0, N)\}, \\ h_{(\ell, N-\ell)}^{(r, N-r)} &= \delta_{r, \ell}, \quad 1 \leq \ell \leq N-1, \\ h_{(\ell, N-\ell)}^{(r, s)} &= 0, \quad 1 \leq \ell \leq N-1, \quad (r, s) \in \{(0, 0), (N, 0), (0, N)\}. \end{aligned} \tag{46}$$

This is the desired linear system. \square

C Continuous mutation accumulation

C.1 Skeleton spectrum

Under continuous mutation accumulation, the expected fixed-time spectrum of the skeleton is given by

$$\mathbb{E}[\tilde{S}_j(\tilde{t}_N)] = (\nu/\lambda_0)N \cdot \int_0^{1-1/N} (1-y)y^{j-1}dy,$$

which is the same as (9) of Proposition 1 with w/q_0 replaced by ν/λ_0 , the effective mutation rate of the continuous-time model. We can use the same proof as in Appendix A, simply replacing the mutation rate wr_0 by ν and noting that $q_0 = \lambda_0/r_0$. However, the expected fixed-size spectrum of the skeleton becomes

$$\mathbb{E}[\tilde{S}_j(\tilde{\tau}_N)|\Omega_\infty] = \begin{cases} (\nu/\lambda_0) \cdot \sum_{k=1}^{N-\max(2,j)} \frac{k}{N-j} \prod_{n=1}^{j-1} (1 - \frac{k}{N-n}), & 1 \leq j \leq N-1, \\ \nu/\lambda_0, & j = N. \end{cases} \quad (47)$$

In the continuous model, mutations occur at rate ν per unit time, and the effective type-2 cell divisions occur at rate λ_0 per unit time. Thus, for $1 \leq k \leq N-1$, the number of mutations that accumulate on level k , prior to the type-2 division that changes levels to $k+1$, has the geometric distribution with support $\{0, 1, 2, \dots\}$ and success probability

$$k\lambda_0/(k\lambda_0 + k\nu) = \lambda_0/(\lambda_0 + \nu).$$

The expected number of mutations per level is therefore

$$(\lambda_0 + \nu)/\lambda_0 - 1 = \nu/\lambda_0,$$

which applies to all levels k with $1 \leq k \leq N-1$. In particular, there are ν/λ_0 ($= w/q_0$) clonal mutations in the continuous model, as opposed to $w p_0/q_0 = w/q_0 - w$ clonal mutations in the discrete model. The reason for this difference is that in the discrete model, the clonal mutations come from the type-1 divisions that occur before the first type-2 division in the process. The first type-2 division adds w mutations, but it also changes levels, so mutations occurring on this division are not clonal. In the continuous model, all mutations occur in between cell divisions, which is why there is no such boundary effect. Similarly, in the discrete model, the very last type-2 division that changes the skeleton size to N adds w mutations on average that each ends up in one cell. This creates the $w\delta_{1,j}$ term in (11) of Proposition 2, which does not occur in (47) for the continuous model. The key differences between mutation accumulation in the two models are diagrammed in Figure 15.

C.2 Total population spectrum

Under continuous mutation accumulation, the expected fixed-time spectrum of the total population is given by

$$\mathbb{E}[S_j(t_N)|Z_0(t_N) > 0] = (\nu/r_0)N \cdot \int_0^{1-1/N} (1-p_0y)^{-1}(1-y)y^{j-1}dy,$$

which is the same as (17) of Proposition 2 with w replaced by ν/r_0 . We can use the same proof as in Appendix B, replacing the mutation rate wr_0 by ν . However, the expected fixed-size spectrum of the total population becomes

$$\mathbb{E}[S_j(\tau_N)|\tau_N < \infty] = (\nu/\lambda_0) \cdot \sum_{k=1}^{N-1} (1-p_0^{N-k})h_{(1,k-1)}^j, \quad 1 \leq j \leq N.$$

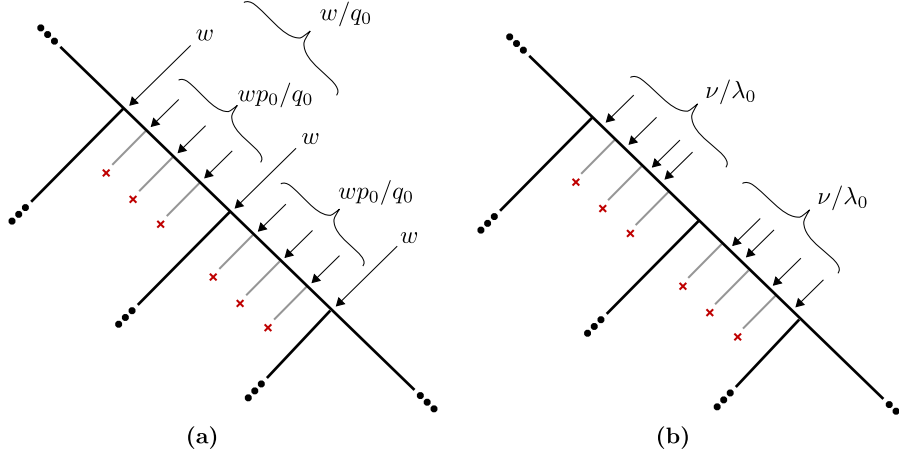


Figure 15: **(a)** In the discrete model of mutation accumulation, mutations coincide with cell divisions. On average, wp_0/q_0 mutations accumulate on type-1 divisions in between two type-2 divisions, and w mutations are added on each type-2 division. This results in $wp_0/q_0 + w = w/q_0$ mutations on average per skeleton level, for all but the first level. **(b)** In the continuous model, all $\nu/\lambda_0 (= w/q_0)$ mutations per level accumulate in between type-2 divisions. The differences between the discrete and continuous model result in boundary effects at $j = 1$ and $j = N$ in the fixed-size spectrum (11) of Proposition 1 that do not appear in the fixed-size result (47) for the continuous model.

In the continuous model, mutations no longer coincide with changes in population level, so instead of counting level changes $\Lambda_{k,k+1}$ as we did in the proof of part (2) of Proposition 2, we need to compute the time spent at level k . We already know from (45) that the number of visits to level k in the embedded discrete-time chain $(X_n)_{n \geq 0}$ has expected value

$$\mathbb{E}_1[\Lambda_k] = \frac{(1+p_0)(1-p_0^{N-k})}{1-p_0^N}.$$

During each visit to state k in the discrete-time chain, the time spent at population level k in the continuous-time process $(Z_0(t))_{t \geq 0}$ is exponentially distributed with rate $k(r_0 + d_0) = kr_0(1 + p_0)$. It follows that the mean time spent on level k for $1 \leq k \leq N - 1$ is

$$\frac{1}{kr_0(1+p_0)} \cdot \frac{(1+p_0)(1-p_0^{N-k})}{1-p_0^N} = \frac{1-p_0^{N-k}}{kr_0(1-p_0^N)}.$$

Since mutations occur at rate $k\nu$ per unit time on level k , we obtain

$$\begin{aligned} \mathbb{E}[S_j(\tau_N) | \tau_N < \infty] &= \frac{1-p_0^N}{q_0} \cdot \sum_{k=1}^{N-1} k\nu \cdot \frac{1-p_0^{N-k}}{kr_0(1-p_0^N)} \cdot h_{(1,k-1)}^{(j,N-j)} \\ &= (\nu/\lambda_0) \cdot \sum_{k=1}^{N-1} (1-p_0^{N-k}) h_{(1,k-1)}^{(j,N-j)}, \end{aligned} \quad (48)$$

where we use that $q_0 = \lambda_0/r_0$. We now have $h_{(1,k-1)}^{(j,N-j)}$ in the sum instead of $h_{(1,k)}^{(j,N-j)}$ in (19) of Proposition 2 since mutations no longer coincide with population level changes. The first equality in (48) can be obtained rigorously using the same argument as in the proof of part (2) of Proposition 2.

D Fixed-time vs. fixed-size spectrum

Here, we present a simple heuristic argument for why the fixed-time and fixed-size spectra of the total population agree on $j \ll N$ when N is large. Conditional on the nonextinction event Ω_∞ , the tumor eventually grows at exponential rate λ_0 . If s is the time it takes to go from population level k to population level N , we can write $k = Ne^{-\lambda_0 s}$ i.e. $e^{\lambda_0 s} = N/k$, following [44]. If we assume s is deterministic, we can write $h_{(1,k)}^{(j,N-j)} \approx p_j(s)$, where $h_{(1,k)}^{(j,N-j)}$ is defined as in Proposition 2 and $(p_j(s))_{j \geq 0}$ is the size-distribution at time s for a single-cell derived clone, we can apply (37) with $e^{\lambda_0 s} = N/k$ to obtain

$$h_{(1,k)}^{(j,N-j)} \approx p_j(s) = \frac{q_0^2 N k}{(N - p_0 k)^2} \cdot \left(\frac{N - k}{N - p_0 k} \right)^{j-1}.$$

Then, observing that $1 - p_0^{N-k} \approx 1$ when $k \ll N$, we can write

$$(w/q_0) \cdot \sum_{k=1}^{N-1} (1 - p_0^{N-k}) \cdot h_{(1,k)}^j \approx (w/q_0) \cdot \int_1^N \frac{q_0^2 N k}{(N - p_0 k)^2} \cdot \left(\frac{N - k}{N - p_0 k} \right)^{j-1}.$$

Using the substitution $y := (N - k)/(N - p_0 k)$ and writing $N - p_0 \approx N$, this becomes the fixed-time spectrum (17) of Proposition 2.

E Derivation of the asymptotic expressions (20) and (21)

Here, we establish the asymptotic expressions (20) and (21) in the main text. To establish (20), fix $0 < p_0 < 1$ and set

$$f_j(k) := p_0^k \cdot \frac{j(j+1)}{(j+k)(j+k+1)}, \quad j \geq 1, k \geq 0.$$

Clearly, $f_j(k) \leq p_0^k$ for all $j \geq 1$ and $k \geq 0$. Since $\sum_{k=0}^{\infty} p_0^k = 1/q_0 < \infty$, it follows from the dominated convergence theorem that

$$\lim_{j \rightarrow \infty} \sum_{k=0}^{\infty} f_j(k) = 1/q_0,$$

from which it follows that

$$wN \cdot \sum_{k=0}^{\infty} \frac{p_0^k}{(j+k)(j+k+1)} \sim (w/q_0)N \cdot 1/(j(j+1)), \quad j \rightarrow \infty.$$

To establish (21), fix $j \geq 1$ and set

$$f_{p_0}(k) := \frac{p_0^k}{(j+k)(j+k+1)}, \quad 0 < p_0 < 1, k \geq 0.$$

Clearly, $f_{p_0}(k) \leq 1/((j+k)(j+k+1))$ for all $0 < p_0 < 1$ and $k \geq 0$. Since

$$\sum_{k=0}^{\infty} \frac{1}{(j+k)(j+k+1)} = \sum_{k=0}^{\infty} \left(\frac{1}{j+k} - \frac{1}{j+k+1} \right) = 1/j < \infty,$$

it follows from the dominated convergence theorem that

$$\lim_{p_0 \rightarrow 1} \sum_{k=0}^{\infty} f_{p_0}(k) = 1/j,$$

from which it follows that

$$wN \cdot \sum_{k=0}^{\infty} \frac{p_0^k}{(j+k)(j+k+1)} \sim wN \cdot 1/j, \quad p_0 \rightarrow 1.$$

F Proof of Proposition 3

Proposition 3. (1) For $0 < p_0 < 1$, the expected total number of mutations in the fixed-time spectrum is given by

$$\begin{aligned}\mathbb{E}[M_1(t_N)|Z_0(t_N) > 0] &= -wN \cdot (1/p_0) \log(q_0 + p_0/N) \\ &\sim -wN \cdot \log(q_0)/p_0, \quad N \rightarrow \infty.\end{aligned}$$

For $p_0 = 0$, $\mathbb{E}[M_1(t_N)|Z_0(t_N) > 0] = w(N-1) \sim wN$ as $N \rightarrow \infty$.

(2) Define \mathcal{S} and A as in Proposition 2. The expected total number of mutations in the fixed-size spectrum is given by

$$\mathbb{E}[M_1(\tau_N)|\tau_N < \infty] = (w/q_0) \cdot \sum_{k=1}^{N-1} (1 - p_0^{N-k}) (1 - h_{(1,k)}^{(0,N)} - h_{(1,k)}^{(0,0)}),$$

where for $(r, s) \in A$, the vector $(h_{(\ell, m)}^{(r, s)})_{(\ell, m) \in \mathcal{S}}$ solves the linear system in Proposition 2. For $p_0 = 0$, $\mathbb{E}[M_1(\tau_N)|\tau_N < \infty] = w(N-1) \sim wN$ as $N \rightarrow \infty$.

Proof. (1) Define $M_j(t) := \sum_{k \geq j} S_k(t)$ as the cumulative number of mutations found in $\geq j$ cells at time t . For fixed $j \geq 1$, by (17) of Proposition 2 and Fubini's theorem, the expected cumulative fixed-time spectrum can be written as

$$\begin{aligned}\mathbb{E}[M_j(t_N)|Z_0(t_N) > 0] &= wN \cdot \sum_{k=j}^{\infty} \left(\int_0^{1-1/N} (1 - p_0 y)^{-1} (1 - y) y^{k-1} dy \right) \\ &= wN \cdot \int_0^{1-1/N} (1 - p_0 y)^{-1} (1 - y) \left(\sum_{k=j}^{\infty} y^{k-1} \right) dy \\ &= wN \cdot \int_0^{1-1/N} (1 - p_0 y)^{-1} y^{j-1} dy \\ &= wN \cdot \sum_{k=0}^{\infty} p_0^k \left(\int_0^{1-1/N} y^{j+k-1} dy \right) \\ &= wN \cdot \sum_{k=0}^{\infty} \frac{p_0^k}{j+k} \left(1 - \frac{1}{N} \right)^{j+k}.\end{aligned}\tag{49}$$

To obtain the desired result, set $j = 1$ in (49) and use that $\sum_{k=1}^{\infty} x^k/k = -\log(1-x)$.

(2) By (19) of Proposition 2,

$$\begin{aligned}\mathbb{E}[M_1(\tau_N)|\tau_N < \infty] &= \sum_{j=1}^N \left((w/q_0) \cdot \sum_{k=1}^{N-1} (1 - p_0^{N-k}) \cdot h_{(1,k)}^{(j, N-j)} \right) \\ &= (w/q_0) \cdot \sum_{k=1}^{N-1} (1 - p_0^{N-k}) \cdot \left(\sum_{j=1}^N h_{(1,k)}^{(j, N-j)} \right),\end{aligned}$$

and the result follows from the fact that $\sum_{(r, s) \in A} h_{(1,k)}^{(r, s)} = 1$. \square

G Derivation of expression (26)

Here, we establish expression (26) in the main text. By (17) of Proposition 2 and Fubini's theorem, we can write

$$\begin{aligned}\mathbb{E}[S_1(t_N)|Z_0(t_N) > 0] &= wN \cdot \int_0^{1-1/N} (1 - p_0 y)^{-1} (1 - y) dy \\ &= wN \cdot \sum_{k=0}^{\infty} p_0^k \left(\int_0^{1-1/N} y^k (1 - y) dy \right) \\ &= wN \cdot \sum_{k=0}^{\infty} p_0^k \left(\frac{1}{k+1} \left(1 - \frac{1}{N} \right)^{k+1} - \frac{1}{k+2} \left(1 - \frac{1}{N} \right)^{k+2} \right) \\ &= wN \cdot \sum_{k=0}^{\infty} \frac{p_0^k}{k+1} \left(1 - \frac{1}{N} \right)^{k+1} - wN \cdot \sum_{k=0}^{\infty} \frac{p_0^k}{k+2} \left(1 - \frac{1}{N} \right)^{k+2}.\end{aligned}\tag{50}$$

Using that $\sum_{k=1}^{\infty} x^k/k = -\log(1-x)$, the former term can be computed as

$$wN \cdot \sum_{k=0}^{\infty} \frac{p_0^k}{k+1} \left(1 - \frac{1}{N}\right)^{k+1} = -wN \cdot (1/p_0) \log(q_0 + p_0/N),$$

and the latter term can be computed as

$$\begin{aligned} wN \cdot \sum_{k=0}^{\infty} \frac{p_0^k}{k+2} \left(1 - \frac{1}{N}\right)^{k+2} &= wN \cdot (1/p_0^2) \sum_{k=0}^{\infty} \frac{p_0^{k+2}}{k+2} \left(1 - \frac{1}{N}\right)^{k+2} \\ &= wN \cdot (1/p_0^2) \left(-\log(q_0 + p_0/N) - p_0(1 - 1/N)\right). \end{aligned}$$

Combining with (50), we obtain

$$\mathbb{E}[S_1(t_N) | Z_0(t_N) > 0] = wN \cdot (1/p_0) \left(1 - 1/N + (q_0/p_0) \log(q_0 + p_0/N)\right),$$

the desired result.

H Laws of large numbers

Here, we present simple calculations in support of the laws of large numbers (28) and (29) in the main text. As stated in the main text, conditional on the nonextinction event Ω_{∞} , $Z_0(t) \sim Y e^{\lambda_0 t}$ almost surely as $t \rightarrow \infty$, where Y has the exponential distribution with mean $1/q_0$ (Theorem 1 of [33]). For the fixed-time spectrum, the number of mutations that accumulate in $[0, t_N]$ and are found in $j \geq 1$ cells at time t_N is then approximately

$$S_j(t_N) \approx \int_0^{t_N} w r_0 \cdot Y e^{\lambda_0 t} \cdot p_j(t_N - t) dt.$$

From (42) in the proof of Proposition 2, we know that

$$\begin{aligned} \int_0^{t_N} w r_0 e^{\lambda_0 t} p_j(t_N - t) dt &= w e^{\lambda_0 t_N} \cdot \int_0^{1 - q_0/(e^{\lambda_0 t_N} - p_0)} (1 - p_0 y)^{-1} (1 - y) y^{j-1} dy \\ &\sim w q_0 N \cdot \int_0^1 (1 - p_0 y)^{-1} (1 - y) y^{j-1} dy, \quad N \rightarrow \infty, \end{aligned}$$

where we use that $e^{\lambda_0 t_N} = q_0 N + p_0$ by the definition of t_N in (15). This implies that

$$S_j(t_N) \approx q_0 Y \cdot wN \cdot \int_0^1 (1 - p_0 y)^{-1} (1 - y) y^{j-1} dy$$

for large N . Note that since Y has the exponential distribution with mean $1/q_0$, $q_0 Y$ has the exponential distribution with mean 1. This suggests (28) in the main text.

For the fixed-size spectrum, note that if N is large, then at time $\tau_N - t$, we can write $Z_0(\tau_N - t) \approx N e^{-\lambda_0 t}$. The number of mutations that accumulate in $[0, \tau_N]$ and are found in $j \geq 1$ cells at time τ_N is then approximately

$$S_j(\tau_N) \approx \int_0^{\tau_N} w r_0 \cdot N e^{-\lambda_0 t} \cdot p_j(t) dt = N e^{-\lambda_0 \tau_N} \cdot \int_0^{\tau_N} w r_0 \cdot e^{\lambda_0 t} \cdot p_j(\tau_N - t) dt.$$

Using (42) from the proof of Proposition 2 again, we can write

$$\int_0^{\tau_N} w r_0 \cdot e^{\lambda_0 t} \cdot p_j(\tau_N - t) dt = w e^{\lambda_0 \tau_N} \cdot \int_0^{1 - q_0/(e^{\lambda_0 \tau_N} - p_0)} (1 - p_0 y)^{-1} (1 - y) y^{j-1} dy,$$

from which it follows that

$$\begin{aligned} S_j(\tau_N) &\approx wN \cdot \int_0^{1 - q_0/(e^{\lambda_0 \tau_N} - p_0)} (1 - p_0 y)^{-1} (1 - y) y^{j-1} dy \\ &\approx wN \cdot \int_0^1 (1 - p_0 y)^{-1} (1 - y) y^{j-1} dy \end{aligned}$$

when N is large. This suggests (29) in the main text.

We finally show that it is straightforward to prove a law of large numbers for a simplified version of our model, in which we assume that the tumor bulk grows deterministically, $Z_0(t) = e^{\lambda_0 t}$, mutant clones arise at stochastic rate r_0 , each mutant clone acquires w mutations on average, and mutant clones grow stochastically. To state the result, let $\hat{S}_j(\tilde{t}_N)$ denote the number of mutations found in $j \geq 1$ cells at time \tilde{t}_N under the simplified model, where \tilde{t}_N is given by (7), i.e. $e^{\lambda_0 \tilde{t}_N} = N$. We want to show that

$$\hat{S}_j(\tilde{t}_N) \sim wN \cdot \int_0^1 (1 - p_0 y)^{-1} (1 - y) y^{j-1} dy, \quad (51)$$

almost surely as $N \rightarrow \infty$. Note that the limit is deterministic since we assume deterministic growth of the tumor bulk. To prove the result, for $0 \leq t \leq \tilde{t}_N$, let $\hat{N}_{j,\tilde{t}_N}(t)$ denote the number of mutant clones created in $[0, t]$ that have size $j \geq 1$ at time \tilde{t}_N . Then $(\hat{N}_{j,\tilde{t}_N}(t))_{0 \leq t \leq \tilde{t}_N}$ is an inhomogeneous Poisson process with rate function $\hat{\lambda}(t) = r_0 e^{\lambda_0 t} p_j(\tilde{t}_N - t)$ and mean function

$$\hat{m}(t) = \int_0^t \hat{\lambda}(s) ds, \quad 0 \leq t \leq \tilde{t}_N.$$

Set $\hat{N}_j(\tilde{t}_N) := \hat{N}_{j,\tilde{t}_N}(\tilde{t}_N)$. By (42) in the proof of Proposition 2, and the fact that $e^{\lambda_0 \tilde{t}_N} = N$,

$$\begin{aligned} \hat{m}(\tilde{t}_N) &= N \cdot \int_0^{1-q_0/(N-p_0)} (1 - p_0 y)^{-1} (1 - y) y^{j-1} dy \\ &\sim N \cdot \int_0^1 (1 - p_0 y)^{-1} (1 - y) y^{j-1} dy, \quad N \rightarrow \infty. \end{aligned}$$

Then, by a simple Poisson concentration inequality, see Theorem 1 of [53],

$$\begin{aligned} \mathbb{P}(|\hat{N}_j(\tilde{t}_N)/\hat{m}(\tilde{t}_N) - 1| > (\hat{m}(\tilde{t}_N))^{-1/3}) &= \mathbb{P}(|\hat{N}_j(\tilde{t}_N) - \hat{m}(\tilde{t}_N)| > (\hat{m}(\tilde{t}_N))^{2/3}) \\ &\leq 2 \exp(-(\hat{m}(\tilde{t}_N))^{1/3}/2(1 + (\hat{m}(\tilde{t}_N))^{-1/3})). \end{aligned}$$

Since $\hat{m}(\tilde{t}_N)$ is of order N as $N \rightarrow \infty$, it follows from the Borel-Cantelli lemma that $\hat{N}_j(\tilde{t}_N)/\hat{m}(\tilde{t}_N) \rightarrow 1$ a.s. as $N \rightarrow \infty$. Now, let W_1, W_2, \dots be i.i.d. nonnegative integer-valued random variables with mean w . We can then choose copies of W_1, W_2, \dots so that

$$\hat{S}_j(\tilde{t}_N) = \sum_{k=1}^{\hat{N}_j(\tilde{t}_N)} W_k.$$

The desired result then follows from the strong law of large numbers.

References

- [1] Motoo Kimura. Genetic variability maintained in a finite population due to mutational production of neutral and nearly neutral isoalleles. *Genetics research*, 11(3):247–270, 1968.
- [2] Richard Durrett. *Probability models for DNA sequence evolution*. Springer Science & Business Media, 2008.
- [3] Motoo Kimura. The number of heterozygous nucleotide sites maintained in a finite population due to steady flux of mutations. *Genetics*, 61(4):893, 1969.
- [4] John FC Kingman. On the genealogy of large populations. *Journal of applied probability*, pages 27–43, 1982.

- [5] John Frank Charles Kingman. The coalescent. *Stochastic processes and their applications*, 13(3):235–248, 1982.
- [6] GA Watterson. On the number of segregating sites in genetical models without recombination. *Theoretical population biology*, 7(2):256–276, 1975.
- [7] Fumio Tajima. Statistical method for testing the neutral mutation hypothesis by dna polymorphism. *Genetics*, 123(3):585–595, 1989.
- [8] Yun-Xin Fu and Wen-Hsiung Li. Statistical tests of neutrality of mutations. *Genetics*, 133(3):693–709, 1993.
- [9] Justin C Fay and Chung-I Wu. Hitchhiking under positive darwinian selection. *Genetics*, 155(3):1405–1413, 2000.
- [10] Kai Zeng, Yun-Xin Fu, Suhua Shi, and Chung-I Wu. Statistical tests for detecting positive selection by utilizing high-frequency variants. *Genetics*, 174(3):1431–1439, 2006.
- [11] Peter Armitage and Richard Doll. The age distribution of cancer and a multi-stage theory of carcinogenesis. *British journal of cancer*, 8(1):1, 1954.
- [12] Peter Armitage and Richard Doll. A two-stage theory of carcinogenesis in relation to the age distribution of human cancer. *British journal of cancer*, 11(2):161, 1957.
- [13] Alfred G Knudson. Mutation and cancer: statistical study of retinoblastoma. *Proceedings of the National Academy of Sciences*, 68(4):820–823, 1971.
- [14] Peter C Nowell. The clonal evolution of tumor cell populations. *Science*, 194(4260):23–28, 1976.
- [15] Cristian Tomasetti, Bert Vogelstein, and Giovanni Parmigiani. Half or more of the somatic mutations in cancers of self-renewing tissues originate prior to tumor initiation. *Proceedings of the National Academy of Sciences*, 110(6):1999–2004, 2013.
- [16] Ivana Bozic, Johannes G Reiter, Benjamin Allen, Tibor Antal, Krishnendu Chatterjee, Preya Shah, Yo Sup Moon, Amin Yaqubie, Nicole Kelly, Dung T Le, et al. Evolutionary dynamics of cancer in response to targeted combination therapy. *elife*, 2:e00747, 2013.
- [17] Rebecca A Burrell, Nicholas McGranahan, Jiri Bartek, and Charles Swanton. The causes and consequences of genetic heterogeneity in cancer evolution. *Nature*, 501(7467):338–345, 2013.
- [18] Bert Vogelstein, Nickolas Papadopoulos, Victor E Velculescu, Shibin Zhou, Luis A Diaz, and Kenneth W Kinzler. Cancer genome landscapes. *science*, 339(6127):1546–1558, 2013.
- [19] Nicholas McGranahan and Charles Swanton. Clonal heterogeneity and tumor evolution: past, present, and the future. *Cell*, 168(4):613–628, 2017.
- [20] Andrea Sottoriva, Haeyoun Kang, Zhicheng Ma, Trevor A Graham, Matthew P Salomon, Junsong Zhao, Paul Marjoram, Kimberly Siegmund, Michael F Press, Darryl Shibata, et al. A big bang model of human colorectal tumor growth. *Nature genetics*, 47(3):209–216, 2015.

- [21] Shaoping Ling, Zheng Hu, Zuyu Yang, Fang Yang, Yawei Li, Pei Lin, Ke Chen, Lili Dong, Lihua Cao, Yong Tao, et al. Extremely high genetic diversity in a single tumor points to prevalence of non-darwinian cell evolution. *Proceedings of the National Academy of Sciences*, 112(47):E6496–E6505, 2015.
- [22] Marc J Williams, Benjamin Werner, Chris P Barnes, Trevor A Graham, and Andrea Sottoriva. Identification of neutral tumor evolution across cancer types. *Nature genetics*, 48(3):238, 2016.
- [23] Subramanian Venkatesan and Charles Swanton. Tumor evolutionary principles: how intratumor heterogeneity influences cancer treatment and outcome. *American Society of Clinical Oncology Educational Book*, 36:e141–e149, 2016.
- [24] Alexander Davis, Ruli Gao, and Nicholas Navin. Tumor evolution: Linear, branching, neutral or punctuated? *Biochimica et Biophysica Acta (BBA)-Reviews on Cancer*, 1867(2):151–161, 2017.
- [25] Thomas O McDonald, Shaon Chakrabarti, and Franziska Michor. Currently available bulk sequencing data do not necessarily support a model of neutral tumor evolution. *Nature genetics*, 50(12):1620–1623, 2018.
- [26] Maxime Tarabichi, Iñigo Martincorena, Moritz Gerstung, Armand M Leroi, Florian Markowetz, Paul T Spellman, Quaid D Morris, Ole Christian Lingjærde, David C Wedge, and Peter Van Loo. Neutral tumor evolution? *Nature genetics*, 50(12):1630–1633, 2018.
- [27] Ivana Bozic, Chay Paterson, and Bartłomiej Waclaw. On measuring selection in cancer from subclonal mutation frequencies. *PLoS computational biology*, 15(9):e1007368, 2019.
- [28] Timon Heide, Luis Zapata, Marc J Williams, Benjamin Werner, Giulio Caravagna, Chris P Barnes, Trevor A Graham, and Andrea Sottoriva. Reply to ‘neutral tumor evolution?’. *Nature genetics*, 50(12):1633–1637, 2018.
- [29] Benjamin Werner, Marc J Williams, Chris P Barnes, Trevor A Graham, and Andrea Sottoriva. Reply to ‘currently available bulk sequencing data do not necessarily support a model of neutral tumor evolution’. *Nature genetics*, 50(12):1624–1626, 2018.
- [30] Marc J Williams, Benjamin Werner, Timon Heide, Christina Curtis, Chris P Barnes, Andrea Sottoriva, and Trevor A Graham. Quantification of subclonal selection in cancer from bulk sequencing data. *Nature genetics*, 50(6):895–903, 2018.
- [31] Khanh N Dinh, Roman Jaksik, Marek Kimmel, Amaury Lambert, Simon Tavaré, et al. Statistical inference for the evolutionary history of cancer genomes. *Statistical Science*, 35(1):129–144, 2020.
- [32] Giulio Caravagna, Timon Heide, Marc J Williams, Luis Zapata, Daniel Nichol, Ketevan Chkhaidze, William Cross, George D Cresswell, Benjamin Werner, Ahmet Acar, et al. Subclonal reconstruction of tumors by using machine learning and population genetics. *Nature Genetics*, 52(9):898–907, 2020.
- [33] Richard Durrett. Branching process models of cancer. In *Branching Process Models of Cancer*, pages 1–63. Springer, 2015.

- [34] Hisashi Ohtsuki and Hideki Innan. Forward and backward evolutionary processes and allele frequency spectrum in a cancer cell population. *Theoretical Population Biology*, 117:43–50, 2017.
- [35] Rick Durrett. Population genetics of neutral mutations in exponentially growing cancer cell populations. *The annals of applied probability: an official journal of the Institute of Mathematical Statistics*, 23(1):230, 2013.
- [36] Ivana Bozic, Jeffrey M Gerold, and Martin A Nowak. Quantifying clonal and subclonal passenger mutations in cancer evolution. *PLoS computational biology*, 12(2):e1004731, 2016.
- [37] Benjamin Werner, Jack Case, Marc J Williams, Ketevan Chkhaidze, Daniel Temko, Javier Fernández-Mateos, George D Cresswell, Daniel Nichol, William Cross, Inmaculada Spiteri, et al. Measuring single cell divisions in human tissues from multi-region sequencing data. *Nature communications*, 11(1):1–9, 2020.
- [38] Siân Jones, Wei-dong Chen, Giovanni Parmigiani, Frank Diehl, Niko Beerenwinkel, Tibor Antal, Arne Traulsen, Martin A Nowak, Christopher Siegel, Victor E Velculescu, et al. Comparative lesion sequencing provides insights into tumor evolution. *Proceedings of the National Academy of Sciences*, 105(11):4283–4288, 2008.
- [39] Neil O’Connell. Yule process approximation for the skeleton of a branching process. *Journal of applied probability*, 30(3):725–729, 1993.
- [40] Natalia L Komarova, Lin Wu, and Pierre Baldi. The fixed-size luria–delbruck model with a nonzero death rate. *Mathematical biosciences*, 210(1):253–290, 2007.
- [41] Stefano Avanzini and Tibor Antal. Cancer recurrence times from a branching process model. *PLoS computational biology*, 15(11):e1007423, 2019.
- [42] Ugo Del Monte. Does the cell number 109 still really fit one gram of tumor tissue? *Cell cycle*, 8(3):505–506, 2009.
- [43] Kevin Leder, Jasmine Foo, Brian Skaggs, Mercedes Gorre, Charles L Sawyers, and Franziska Michor. Fitness conferred by bcr-abl kinase domain mutations determines the risk of pre-existing resistance in chronic myeloid leukemia. *PloS one*, 6(11):e27682, 2011.
- [44] Yoh Iwasa, Martin A Nowak, and Franziska Michor. Evolution of resistance during clonal expansion. *Genetics*, 172(4):2557–2566, 2006.
- [45] Amaury Lambert. The allelic partition for coalescent point processes. *arXiv preprint arXiv:0804.2572*, 2008.
- [46] David Cheek, Tibor Antal, et al. Mutation frequencies in a birth–death branching process. *The Annals of Applied Probability*, 28(6):3922–3947, 2018.
- [47] Jack Kuipers, Katharina Jahn, Benjamin J Raphael, and Niko Beerenwinkel. Single-cell sequencing data reveal widespread recurrence and loss of mutational hits in the life histories of tumors. *Genome research*, 27(11):1885–1894, 2017.

- [48] David A Kessler and Herbert Levine. Large population solution of the stochastic luria–delbrück evolution model. *Proceedings of the National Academy of Sciences*, 110(29):11682–11687, 2013.
- [49] Peter Keller and Tibor Antal. Mutant number distribution in an exponentially growing population. *Journal of Statistical Mechanics: Theory and Experiment*, 2015(1):P01011, 2015.
- [50] Robert C Griffiths and Anthony G Pakes. An infinite-alleles version of the simple branching process. *Advances in applied probability*, pages 489–524, 1988.
- [51] Nicolas Champagnat, Amaury Lambert, and Mathieu Richard. Birth and death processes with neutral mutations. *International Journal of Stochastic Analysis*, 2012, 2012.
- [52] Xiaowei Wu and Marek Kimmel. Modeling neutral evolution using an infinite-allele markov branching process. 2013.
- [53] C. Cannone. A short note on Poisson tail bounds. 2017. <http://www.cs.columbia.edu/~ccannonne/files/misc/2017-poissonconcentration.pdf>.